Review

A Fascinating Trip into Iron and Copper Dyes for DSSCs

Luca Mauri, Alessia Colombo, Claudia Dragonetti and Francesco Fagnani *

Department of Chemistry, University of Milan, UdR-INSTM, Via Golgi 19,
I-20133 Milano, Italy
* Correspondence: francesco.fagnani@unimi.it

Abstract: The production of electricity in a greener and more sustainable way by employing renewable sources is a great challenge in modern times. Photovoltaic systems represent an important possibility because sunlight is the most abundant renewable source. In this review article, recent studies (from 2018 to the present) involving novel iron and copper complexes employed as dyes in Dye-Sensitized Solar Cells (DSSCs) are reported; mono- and bimetallic Fe complexes, Cu-based dyes, and devices presenting both metals are discussed, together with the performances of the DSSCs reported in the papers and the corresponding values of the main parameters employed to characterize such solar cells. The feasibility of DSSCs employing copper and iron dyes, alone or in combination with other earth-abundant metals, is demonstrated. The proper optimization of the sensitizers, together with that of the electrolyte and of the semiconducting layer, will likely lead to the development of highly performing and cheap photovoltaic devices for future applications on a much larger scale.

1. Introduction

In the face of climate change and global warming, many solutions for energy conversion have been developed with the aim of producing electricity in a greener and more sustainable way by employing renewable sources. Among them, photovoltaic systems represent an important solution because sunlight is the most abundant renewable resource [1] and photovoltaic devices can easily be integrated in buildings, providing high conversion efficiencies.

Particularly interesting are the so-called Dye-Sensitized Solar Cells (DSSCs), first described by Grätzel and O'Regan in 1991 [2]: these devices (schematized in Figure 1) are based on a sensitizer (an organometallic or coordination complex, or purely organic compound) adsorbed on the surface of a semiconductor film (usually titanium dioxide), which is deposited onto a photoanode made of a conductive oxide, such as fluorine-doped tin oxide (FTO). The cathode is often constituted by a layer of FTO on which a counter electrode, usually made of Platinum or graphite, is deposited. Between the anode and the cathode, an electrolytic solution containing a redox couple—usually the I^-/I_3^- type—and some additives (such as 4-*tert*-butylpyridine, TBP) are placed.
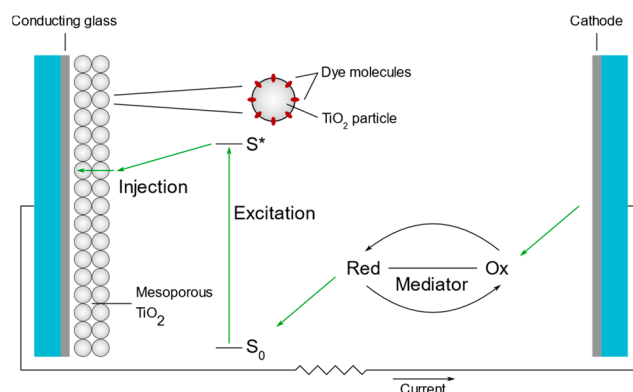
Figure 1. Simplified scheme and working principle of a DSSC.

When sunlight hits the cells, it is absorbed by the dye molecule, which reaches an excited state from which the injection of an electron in the conduction band of the TiO$_2$ layer occurs. The injected electron reaches the photoanode and consequently the cathode by passing through an external circuit; there, it is recombined with the oxidized species of the redox mediator to create the reduced form. This species reacts with the oxidized dye, reducing it and preparing the molecule for another cycle.

Among the wide variety of dyes employed as sensitizers in DSSCs, one can use both organic compounds, such as **D205**, and coordination compounds, such as **N719** and **N3** (structures in Figure 2). Record efficiencies overcoming 20% [3] were obtained with the dye **N719**, which is often employed as a term of comparison in studies describing novel dyes for DSSCs. Up to now, many examples of Ru(II) dyes have been tested, at first, with a structure similar to that of **N719**, and later, avoiding the presence of NCS ligands [4–13].
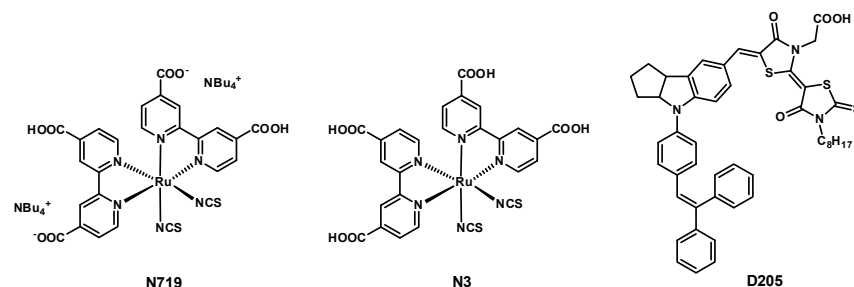
Figure 2. Structure of dyes **N719**, **N3,** and **D205**.

Dyes such as **N719** present chelating bipyridine ligands functionalized with carboxyl groups, which are necessary to anchor these molecules onto the titania layer, and two monodentate thiocyanate ligands. The main problems arising from the use of Ru(II) complexes such as **N719** are the replacement of the thiocyanate groups by other species often present in the redox mediator (such as 4-*tert*-butylpyridine), its scarcity, and the high cost. To find a solution, many iron and copper complexes have been proposed as an alternative to the conventional Ru(II)-based ones because Cu and Fe are cheaper and much more abundant than Ru. The goal of this review is to retrace the development of copper and iron complexes as sensitizers for DSSCs from 2018 to the present, inspired by the excellent review of C. Housecroft et al. [14], and to show the main results obtained by employing them, including their possible use in combination with other cheap and abundant metal cations, such as Zn and Ni cations.

2. Iron Monometallic and Bimetallic Complexes

This section reports the recent studies, from 2018 to present, in which novel iron and copper complexes were employed as dyes in DSSCs. Not only the structure and the performances of the cells were considered, but also other important aspects such as the shape of the UV–Vis spectra and the position of the highest occupied molecular orbital (HOMO) and lowest unoccupied molecular orbital (LUMO) levels.

2.1. Iron Complexes

Iron complexes as sensitizers for DSSCs were first described in 2002 by Ferrere [15], who employed 2,2′-bipyridine-4,4′-dicarboxylic acid and cyanides as ligands. Here, we discuss the most recent papers published in the field of iron complexes as sensitizers in DSSCs.

In 2018, Bera and Chatterjee et al. [16] published and tested two new ferrocene-cyanovinyl sensitizers (complexes **1a** and **1b**, structure in Figure 3). The two dyes were rather similar, except for the presence of a single acceptor group (cianovinyl chain) in complex **1a** and two acceptors in complex **1b**.
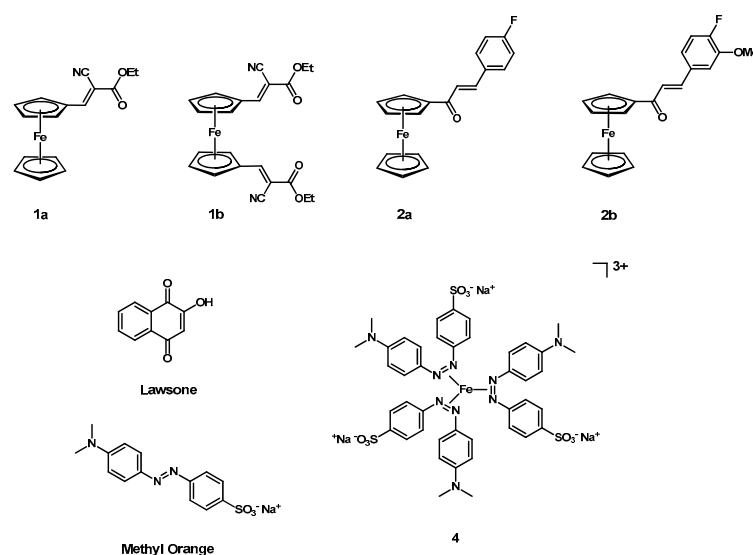
Figure 3. Structure of dyes **1a–b**, **2a–b** and **4**, of Lawsone and of Methyl Orange.

Compound **1a**, due to the presence of only one acceptor, showed a reversible oxidation process (+0.61 V vs. Saturated Calomel Electrode (SCE)), whereas compound **1b** was oxidized with greater difficulty (+0.87 V vs SCE) because of the presence of two cianovinyl chains. Dye **1a** also showed a higher molar extinction coefficient (ε) than **1b**.

Compounds **1a** and **1b** were used as sensitizer DSSCs, employing mesoporous TiO_2 on FTO as a support. The peculiarity of the cells fabricated with **1a** and **1b** stemmed from the absence of a redox mediator thanks to their ability to act both as a dye and a redox couple. The devices were tested under 1 Sun irradiation in air (Reference Air Mass 1.5 Spectra, AM 1.5 G, 100 mW cm^{-2}) and their characteristics are summarized in Table 1 entries 1–2. Density Functional Theory (DFT) calculations on the neutral and the oxidized species showed that the molecular orbitals of the oxidized species were more stable than the Pt work function. The optimization of the oxidized species not only aided the regeneration of the dye by the Pt cathode, but also reduced the recombination processes and made the cyanovinyl-ferrocene dyes interesting candidates for electrolyte-free DSSCs.

Table 1. Photovoltaic data of DSSCs produced with dyes **1a–b**, **2a–b**, and **3a–g**, **4** [1].

Entry	Dye	Redox Couple	J_{SC} (mA cm^{-2})	V_{OC} (V)	FF	η (%)	η_{rel} [2] (%)	Ref.
1	**1a** [3]	Absent [4]	0.410	0.763	0.35	0.10		[16]
2	**1b** [3]	Absent [4]	0.039	0.841	0.28	9.18×10^{-3}		[16]
3	**2a**	I^-/I_3^- [5]	0.606	0.593	58.70	0.211	41.21	[17]
4	**2b**	I^-/I_3^- [5]	0.776	0.601	52.70	0.246	48.05	[17]
5	**N719**	I^-/I_3^- [5]	1.153	0.626	70.90	0.512		[17]
6	Lawsone ligand [5]	I^-/I_3^-	2.21	0.66	0.64	0.94	0.31	[18]
7	**3a** [6]	I^-/I_3^-	2.48	0.66	0.65	1.08	0.36	[18]
8	**3b** [6]	I^-/I_3^-	2.86	0.66	0.65	1.23	0.40	[18]
9	**3c** [6]	I^-/I_3^-	3.27	0.66	0.65	1.41	0.46	[18]
10	**3d** [6]	I^-/I_3^-	3.77	0.66	0.62	1.54	0.51	[18]
11	**3e** [6]	I^-/I_3^-	3.96	0.66	0.62	1.63	0.54	[18]
12	**3f** [6]	I^-/I_3^-	4.43	0.66	0.65	1.90	0.63	[18]
13	**3g** [6]	I^-/I_3^-	4.92	0.66	0.65	2.11	0.69	[18]
14	**N719** [6]	I^-/I_3^-	5.40	0.86	0.65	3.04		[18]
15	Lawsone ligand [7]	I^-/I_3^-	2.39	0.68	0.65	1.06	0.24	[18]
16	**3a** [7]	I^-/I_3^-	3.06	0.68	0.65	1.39	0.32	[18]
17	**3b** [7]	I^-/I_3^-	3.41	0.68	0.66	1.53	0.35	[18]
18	**3c** [7]	I^-/I_3^-	3.71	0.68	0.66	1.67	0.38	[18]
19	**3d** [7]	I^-/I_3^-	4.26	0.68	0.66	1.93	0.44	[18]
20	**3e** [7]	I^-/I_3^-	4.50	0.68	0.66	2.02	0.46	[18]
21	**3f** [7]	I^-/I_3^-	5.32	0.68	0.66	2.39	0.54	[18]
22	**3g** [7]	I^-/I_3^-	6.33	0.68	0.66	2.85	0.65	[18]
23	**N719** [7]	I^-/I_3^-	7.80	0.86	0.66	4.40		[18]
24	Methyl Orange [8]	I^-/I_3^- [9]	3.00	0.15	0.83	0.756		[19]
25	**4** [8]	I^-/I_3^- [9]	3.75	0.15	1.00	1.137		[19]

[1] using FTO as conductive oxide, TiO_2 as semiconductor, Pt as counter-electrode, and under AM 1.5 G-simulated light source (100 mW cm^{-2}) if not differently specified. [2] η_{rel}: relative efficiency with respect to **N719**. [3] 0.01 M dye in dichloromethane (DCM). [4] compounds **1a–b** acted both as dyes and redox mediators, and the cells were fabricated without a redox electrolyte solution. [5] Solaronix Iodolyte AN-50. [6] TiO. Nanoparticles. [7] TiO_2 nanofibers. [8] 10^{-5} M. [9] KI_3.

In 2020, Arshad et al. [17] presented the two ferrocenyl chalcones **2a** and **2b** (structures in Figure 3). These complexes differed only in the substituent in position 3 of the phenyl ring, namely, a hydrogen atom in compound **2a** and an electron-donating methoxy group in compound **2b**.

Dye **2a** showed slightly lower HOMO and LUMO levels and a smaller gap than **2b** (3.37 eV against 3.52 eV) because of the absence of the methoxy group. Compound **2b** also had a higher absorbance than **2a**. The absorption maximum was significantly red-shifted of 26 nm and, even in this case, it was a consequence of the presence of an electron-donating group instead of a simpler hydrogen atom. The structural analysis of dye **2b** also showed that the methoxy group made it more planar than its counterpart **2a**. This particular characteristic was reflected in a more efficient intramolecular charge transfer.

The photovoltaic performances of the DSSCs fabricated with dyes **2a** and **2b**, and with the reference **N719,** are listed in Table 1, entries 3-5. From their characterization, which was carried out under AM 1.5 G irradiation, it emerged that both the Short Circuit Current (J_{SC}) and the Open Circuit Voltage (V_{OC}) followed the trend **2a** < **2b** < **N719**; the higher values observed for **2b** were associated with the higher degree of planarity. The case of the Fill Factor was different (FF), as it was higher in the case of the device containing **2a** than **2b;** in fact, **2a** was characterized by a stronger absorption than that of **2b**. However, **N719** showed a much higher FF than **2a–b** because the novel dyes did not contain any anchoring carboxylic group. Despite their lower conversion efficiencies than that of **N719**, optimizing **2a** and **2b** will result in the enhancement of the performances of DSSCs based on ferrocenyl-chalcones and in the development of suitable candidates for this application.

In 2020, Sreelatha et al. [18] published seven new metal lawsone-based complexes **3a–g**. Lawsone (structure in Figure 3), also known as 2-hydroxy-1,4-naphthoquinone, was

considered because of its ease of functionalization, higher stability, and the improved performances of the devices containing its complexes. In particular, the synthesized ligand resulted from a Mannich reaction between lawsone, benzaldehyde, and butan-1-amine, and it was employed to produce complexes of Mn(II), Zn(II), Ni(II), Co(II), Cu(II), Fe(II), and Cr(III).

The UV–Vis characterization was carried out using dimethyl sulphoxide (DMSO) as a solvent: the lawsone ligand showed two absorption bands around 300 and 450 nm, while those of its complexes were around 350 and 650 nm. In general, the absorbance followed the trend **3g** < **3a** < **3d** < **3b** < **3c** < **3f** < **3e**.

Two different types of photovoltaic devices, the former using TiO_2 nanoparticles, the latter employing TiO_2 nanofibers as photoanode, were assembled with the lawsone, each complex, and the reference dye **N719** (data in Table 1, entries 6–23). While the observed V_{OC} and FF were almost constant (except for the higher V_{OC} of **N719**), the J_{SC} showed increasing values passing from the lawsone to **3a–g** (Fe(II) was second only to Cr(III)). Moreover, the use of TiO_2 nanofibers instead of nanocrystalline TiO_2 was useful for increasing the energy conversion. It was also demonstrated that titania nanofibers allowed for a slower reduction of the DSSC efficiency (η) over time. Despite the higher efficiency of **N719**, the lawsone Fe(II) complex **3f** represented an interesting candidate for applications in DSSCs and a remarkable improvement with respect to the simple lawsone molecule.

In 2020, Setyawati et al. [19] prepared a new methyl orange Fe(II) complex not only to increase the ability of this ligand as light absorber, but to reach an enhanced stability of the resulting compound (see Figure 3).

The UV–Vis characterization of compound **4** showed a noticeable blue shift from 464 nm to 420 nm of the absorption maximum wavelength when compared to methyl orange. In addition, the charge transfer phenomenon was significantly blue-shifted, from 278 nm to 262 nm, after the metal insertion, representing a clear indication of an improved electron transport in the photovoltaic device.

Methyl orange and compound **4** were employed for the production of DSSCs using TiO_2 as a photoanode. The photovoltaic performances are listed in Table 1, entries 24–25, and an evident improvement with respect to the methyl orange was observed. The synthesis of metal complexes using such simple ligands can represent an interesting way to develop greener production of electricity.

In 2021, Arshad et al. [20] published two novel ferrocenyl chalcones, compounds **5a** and **5b** (structures in Figure 4), with different aromatic rings. Differently from the work of Arshad et al. [17], dyes **5a** and **5b** contained a 5-ethylfuran-2-yl and a 2,2'-bithiophen-5-yl moiety, respectively.
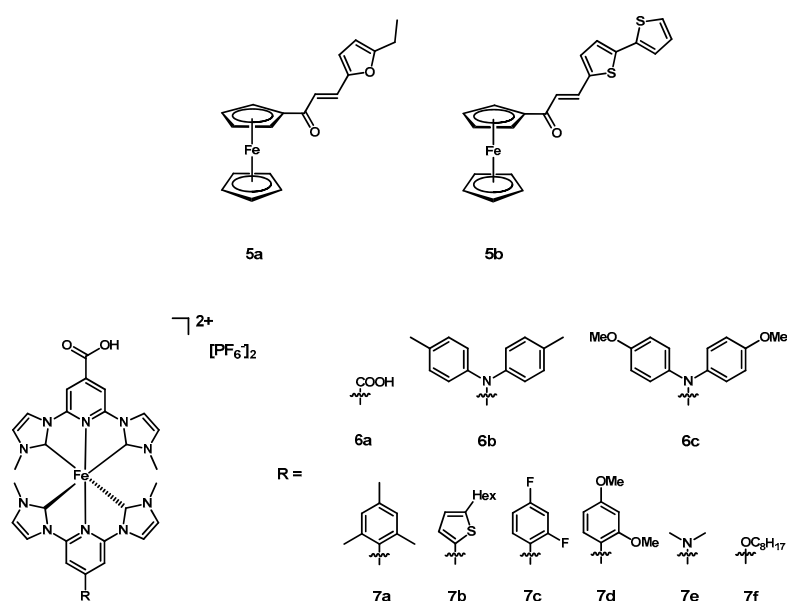
Figure 4. Structure of dyes **5a–b**, **6a–c,** and **7a–f**.

The UV–Vis spectra of **5a** and **5b** showed a broad absorption band at 486 and 483 nm, and more intense bands were observed at 345 nm for **5a** and 385 nm for **5b**. A stronger red shift was observed for the latter, which was attributable to the presence of two thiophene rings in this complex. From DFT calculations, it emerged that the HOMO–LUMO gaps were 3.488 eV and 3.153 eV for **5a** and **5b**; hence, the second one was characterized by an easier charge transfer process. In any case, the HOMO levels of **5a** and **5b** remained lower than the I^-/I_3^- couple redox potential. Therefore, it could be used as redox mediator for restoring both the oxidized dyes.

Compounds **5a** and **5b** were incorporated in DSSC devices and tested under AM 1.5G irradiation conditions. The photovoltaic performances of the DSSCs containing them, summarized in Table 2, entries 1–2, were higher for **5b** than for **5a**. Similar to complexes **2a** and **2b**, the higher planarity of **5a** resulted in a more efficient intramolecular charge transfer, and hence in a better electron injection in the TiO_2 layer. Despite the low conversion efficiency, the higher planarity of **5b** made it an interesting starting point for synthesizing new ferrocenyl chalcones with various substituents and improved performances.

Table 2. Photovoltaic data of DSSCs produced with dyes **5a–b**, **6a–c**, **7a–f**, **8a–c**, **9**, and **10a–b** [1].

Entry	Dye	Redox Couple	J_{SC} (mA cm^{-2})	V_{OC} (V)	FF	η (%)	η_{rel} (%)	Ref.
1	**5a** [2]	I^-/I_3^- [3]	0.036	0.191	50.20	0.0034		[20]
2	**5b** [2]	I^-/I_3^- [3]	0.132	0.491	63.40	0.0412		[20]
3	**6a** [4,5]	I^-/I_3^- [6]	2.09	0.466	0.752	0.73		[21]
4	**6b** [4,5]	I^-/I_3^- [6]	3.52	0.512	0.724	1.31		[21]
5	**6c** [4,5]	I^-/I_3^- [6]	3.23	0.416	0.694	0.93		[21]
6	**7a** [7,8]	I^-/I_3^- [9]	6.03 ± 0.34	0.47 ± 0.01	0.59 ± 0.01	1.68 ± 0.14		[22]
7	**7b** [7,8]	I^-/I_3^- [9]	6.07 ± 0.45	0.43 ± 0.01	0.61 ± 0.03	1.58 ± 0.13		[22]
8	**7c** [7,8]	I^-/I_3^- [9]	5.81 ± 0.41	0.47 ± 0.01	0.57 ± 0.03	1.56 ± 0.18		[22]
9	**7d** [7,8]	I^-/I_3^- [9]	6.11 ± 0.46	0.39 ± 0.01	0.49 ± 0.02	1.17 ± 0.15		[22]
10	**7e** [7,8]	I^-/I_3^- [9]	6.80 ± 0.17	0.47 ± 0.02	0.57 ± 0,02	1.83 ± 0.10		[22]
11	**7f** [7,8]	I^-/I_3^- [9]	5.20 ± 0.33	0.35 ± 0.01	0.61 ± 0.02	1.11 ± 0.12		[22]
12	**6a** [7,8]	I^-/I_3^- [9]	5.60 ± 0.29	0.44 ± 0.01	0.56 ± 0.01	1.39 ± 0.13		[22]
13	**7c** [8,10]	I^-/I_3^- [9]	4.87 ± 0.31	0.43 ± 0.01	0.59 ± 0.02	1.24 ± 0.10		[22]
14	**7d** [8,10]	I^-/I_3^- [9]	4.82 ± 0.31	0.37 ± 0.02	0.51 ± 0.02	0.91 ± 0.12		[22]
15	**7e** [8,10]	I^-/I_3^- [9]	5.59 ± 0.18	0.44 ± 0.01	0.58 ± 0.01	1.43 ± 0.10		[22]
16	**6a** [8,10]	I^-/I_3^- [9]	4.30 ± 0.30	0.43 ± 0.01	0.59 ± 0.03	1.10 ± 0.09		[22]
17	**7c** [8,10]	I^-/I_3^- [9]	5.41 ± 0.30	0.46 ± 0.01	0.58 ± 0.01	1.44 ± 0.10		[22]
18	**7d** [8,10]	I^-/I_3^- [9]	5.45 ± 0.10	0.39 ± 0.01	0.47 ± 0.04	1.00 ± 0.15		[22]
19	**7e** [8,10]	I^-/I_3^- [9]	6.33 ± 0.30	0.46 ± 0.01	0.57 ± 0.01	1.65 ± 0.12		[22]

#	Dye	Redox						Ref
20	**6a** [8,10]	I⁻/I3⁻ [9]	5.22 ± 0.18	0.45 ± 0.01	0.57 ± 0.02	1.35 ± 0.07		[22]
21	**8a** [11,12]	I⁻/I3⁻ [13]	3.55	0.44	0.6	0.94 ± 0.11	26.33	[23]
22	**8b** [11,12]	I⁻/I3⁻ [13]	2.69	0.46	0.63	0.78 ± 0.08	21.85	[23]
23	**8c** [11,14]	I⁻/I3⁻ [13]	3.95	0.49	0.61	1.18 ± 0.10	33.05	[23]
24	**6a** [11,14]	I⁻/I3⁻ [13]	3.64	0.45	0.62	1.02 ± 0.11	28.57	[23]
25	**N719** [11,15]	I⁻/I3⁻ [13]	12.84	0.48	0.58	3.57 ± 0.34		[23]
26	**8a** [11,12]	I⁻/I3⁻ [16]	3.89	0.43	0.57	0.95 ± 0.09	25.82	[23]
27	**8b** [11,12]	I⁻/I3⁻ [16]	2.90	0.45	0.62	0.81 ± 0.10	22.01	[23]
28	**8c** [11,14]	I⁻/I3⁻ [16]	4.44	0.45	0.64	1.27 ± 0.12	34.51	[23]
29	**6a** [11,14]	I⁻/I3⁻ [16]	4.38	0.43	0.59	1.11 ± 0.17	30.16	[23]
30	**N719** [11,15]	I⁻/I3⁻ [16]	12.87	0.50	0.50	3.68 ± 0.52		[23]
31	**6a** [14]	I⁻/I3⁻ [13]	4.02	0.49	0.58	1.14 ± 0.07		[23]
32	**8c** [14]	I⁻/I3⁻ [13]	4.26	0.51	0.59	1.29 ± 0.09		[23]
33	**8c** [14]	I⁻/I3⁻ [16]	4.98	0.47	0.62	1.44 ± 0.07		[23]
34	**NBB** [17,18]	I⁻/I3⁻ [19]	0.0240	0.218	0.7844	0.0083		[24]
35	**9** [17,18]	I⁻/I3⁻ [19]	0.1418	0.363	0.8887	0.0925		[24]
36	**10a**		12.91	0.710	0.64	5.88	93.04	[25]
37	**10b**		9.21	0.690	0.63	4.04	63.92	[25]
38	**N719** [20]		16.44	0.638	0.60	6.32		[25]

[1] using FTO as conductive oxide, TiO_2 as semiconductor, Pt as counter-electrode, and under AM 1.5G-simulated light source (100 mW cm^{-2}) if not differently specified. [2] 0.02 M + 0.002 M chenodeoxycholic acid (CDCA) in ACN. [3] Solaronix Iodolyte AN-50. [4] Nippon sheet glass; 8 Ω sheet resistance. [5] 0.2 mM dye in can; then 0.5 mM CDCA in ACN. [6] 0.1 M LiI + 0.05 M I_2 + 0.6 M 1,2-dimethyl-3-propylimidazolium iodide (DMPII) in 3-methoxypropionitrile (MPN). [7] DSSC fabricated with a 20 μm TiO_2 layer. [8] PEDOT counter electrode. [9] 0.1 M LiI + 0.6 M 1-methyl-3-propylimidazolium iodide (PMII) + 0.1 M I_2 + 0.1 M MgI_2 + 0.1 M guanidinium thiocyanate (GuNCS) + 0.1 M TBAI in ACN. [10] DSSC fabricated with a 16 μm TiO_2 layer. [11] PEDOT counter electrode. [12] 0.05 M in ACN. [13] 0.1 M LiI + 0.6 M PMII + 0.1 M I_2 + 0.1 M MgI_2 + 0.1 M GuNCS in ACN. [14] 0.02 mM dye + 0.04 mM CDCA in ACN. [15] 0.02 mM in ethanol (EtOH). [16] 0.1 M LiI + 0.6 M PMII + 0.1 M I_2 + 0.1 M MgI_2 + 0.1 M GuNCS + 0.1 M TBAI in ACN. [17] Graphite counter electrode. [18] 0.1 mM dye. [19] KI_3. [20] 10^{-4} M dye in ACN:*tert*-butanol (*t*-BuOH).

In 2021, Freitag, Lomoth, Persson, and Wärnmark et al. [21] synthesized and tested three iron-N-heterocyclic carbene (NHC) complexes bearing C^N^C ligands (i.e., pyridine-2,6-diyl)bis(methylimidazole-2-ylidene). Dye **6a** contained two identical ligands with an anchoring carboxylicic group. In contrast, **6b** and **6c** were heteroleptic complexes containing an anchoring and an electron-donor ligand (see Figure 4).

The UV–Vis spectra of **6a–c** were recorded in a buffer system consisting of 0.1 M tetrabutylammonium methanesulfonate and 0.1 M methanesulfonic acid in acetonitrile (ACN) to guarantee the presence of solely the protonated species. The spectra consisted of two absorption bands, the first between 400–430 nm, the other one, more intense, at 500-550 nm, with a tail extended to 600 nm. Compound **6a** exhibited a higher molar extinction coefficient (2.3×10^4 M^{-1} cm^{-1}; absorption maximum (λ_{max}) 515 nm) than compounds **6b** and **6c** (1.6×10^4 M^{-1} cm^{-1} and λ_{max} 511 nm, and 1.4×10^4 M^{-1} cm^{-1} and λ_{max} 512 nm, respectively). Dye **6b** had a slightly higher absorbance than **6c** in the whole visible spectrum. DFT calculations showed a destabilization of both the HOMO and LUMO when a ligand bearing an electron-rich aniline was present, and a remarkable stabilization was observed in the case of compound **6a** because of the two carboxylicic groups. Nevertheless, the stabilization arising from the anchoring ligand was stronger than the destabilization; hence, the LUMO was extended preferentially over this ligand.

Compounds **6a–c** were employed as sensitizers for DSSCs because of their ability to inject electrons into the TiO_2 layer (see Table 2, entries 3–5). The chosen redox couple was I⁻/I3⁻. Dye **6b** showed the best performances, followed by **6c** and **6a**. Particularly interesting were complexes **6b** and **6c** because their improved performances with respect to **6a** were associated with their push–pull character, which conferred to them a higher directionality of charge separation. The LUMO was directed towards the TiO_2 layer because of its position over the anchoring ligand. The presence of two methoxy groups in dye **6c** as opposed to the methyl ones in **6b** resulted into a slower regeneration of the oxidized dye,

and this was probably due to the shorter electron lifetime in the devices containing **6c**. Rather low conversion efficiencies were obtained, but the higher performances of the heteroleptic dyes **6b** and **6c** indicated a clear way to improve these photovoltaic cells employing abundant and cheap metals such as iron.

Six other NHC heteroleptic complexes, i.e., compounds **7a–f** (see Figure 4), were produced, tested, and compared with **6a** by Pastore, Caramori, and Gros et al. [22] in 2021. Differently from complexes **6a–c**, both electron-withdrawing and electron-donating groups were incorporated in the non-anchoring ligand.

The UV–Vis spectra of **7a–c**, and **7e** had a broad absorption band between 410 and 460 nm, while it was even more red-shifted to 450–600 nm in the case of **7d** and **7f**. A less intense band was observed around 400 nm, and a third absorption peak was observed in the near UV range around 300 nm. The electrochemical characterization showed that a suitable redox couple for **7a–f** was I^-/I_3^- because of its efficient ability to regenerate the oxidized dye.

Dyes **7a–f** were tested in DSSC devices using TiO_2 as semiconductor, I^-/I_3^- as electrolytes, and under AM 1.5G illumination conditions. The redox mediator solution also contained Mg^{2+} cations for a better electronic coupling between the dye and the titania conduction band. Several tests were carried out (data in Table 2, entries 6–20) working with a different thickness of the TiO_2 layer, with or without a top scattering layer for an increased optical path of the photons in the semiconductor. The best results were obtained when compound **7e** was deposited onto a 20 μm TiO_2 sheet in the presence of the top scattering layer (in general, better results were obtained with a thicker titania film in the presence of the scattering layer). In addition, in this case, the heteroleptic NHC complexes demonstrated superior performances compared to the homoleptic complexes.

In the same year, Pastore, Caramori, and Gros et al. [23] synthesized three other heteroleptic Fe(II) NHC complexes. Dyes **8a–c** (structures in Figure 5) were characterized by different anchoring ligands containing different spacers between the pyridine and the carboxylic group. The same non-anchoring ligand, namely, 2,6-bis(3-methyl-1*H*-3λ^4-imidazol-1-yl)pyridine, was employed for each complex. These sensitizers were compared with compound **6a**, containing two simple anchoring carboxylic groups.
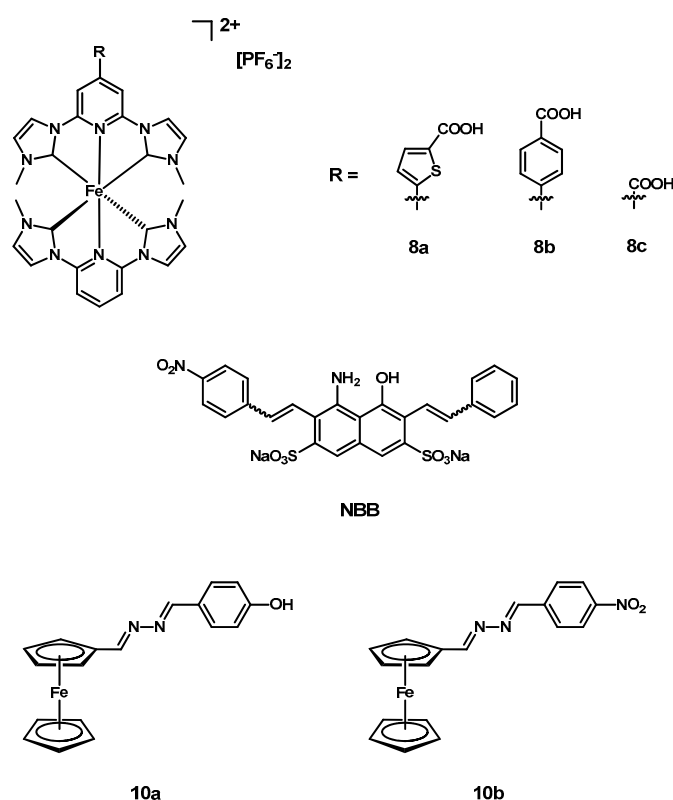
Figure 5. Structure of dyes **8a–c** and **10a–b**, and of Naphthol Blue-Black.

The absorption spectra showed three distinct bands in the regions 250–330 nm, 340–420 nm, and 420–460 nm. The molar extinction coefficients measured in the methanol (MeOH) of **8a** and **8b** (16,725 and 15,306 M^{-1} cm^{-1}) were higher than that of **8c** (12,375 M^{-1} cm^{-1}) since a thiophene or phenyl ring extended the π-system. The oxidation potentials vs. SCE for the dyes **8a–c** and **C1** were 0.74 V, 0.70 V, 0.82 V, and 0.85 V, respectively; **8a** and **8b** showed lower oxidation potentials because of the more extended π-conjugation. In any case, the I^-/I_3^- redox couple was suitable for an efficient dye regeneration. In addition, the excited state oxidation potentials (−1.49 V, −1.62, and −1.57 mV for **8a–c**) were studied and each dye was able to inject electrons in the conduction band of TiO_2.

The photovoltaic performances of the DSSCs assembled using TiO_2 and compounds **8a-c** together with I^-/I_3^- (containing or omitting tetrabutylammonium iodide, abbreviated as TBAI) were tested under AM 1.5G irradiation conditions, employing poly(3,4-ethylene-dioxythiophene) (PEDOT) or Pt counter electrodes (data in Table 2, entries 21–33). The J_{SC} values were in the range between 2.50 and 4.00 mA cm^{-2}. Slightly higher values of the photocurrent and efficiency were observed with the redox solution containing TBAI, even if its role was not fully understood. More constant were the values of V_{OC} and FF. A major improvement was observed when Pt was used as counter electrode instead of PEDOT. Despite the lower molar extinction coefficient of **8c,** it was a better dye than **8a** and **8b** because its less extended π-conjugation allowed for a more efficient electron injection. Dyes **8a–c** provided an interesting demonstration of how to improve the photovoltaic performances of Fe(II)-based DSSCs by developing the anchoring ligand, although their performances were still not comparable to those of **N719**.

In 2021, Setyawati et al. [24] synthesized a new Fe(II) complex **9** using the commercial dye Naphthol Blue Black (NBB, see Figure 5). This ligand was chosen due to its light-harvesting ability, especially thanks to its strong absorption band in the UV range and because its anionic character should guarantee a higher efficiency compared to cationic ligands.

The UV–Vis spectrum of complex **9** was compared to that of the ligand alone: a new absorption band at 273.5 nm was observed because of the presence of the metal center, even if it was much lower than the absorption bands of NBB. The anionic complex **9** had a higher conductivity than the solvent (59.6 μS vs. 1.42 μS of Aqua Bidest®), and the simple ionization was a clear indicator of a faster and continuous electron transfer process.

The photovoltaic performances of NBB and **9** (summarized in Table 2, entries 34–35) were tested using a titania layer and I^-/I_3^- as a redox couple. Similar to complex **4**, compound **9** showed a higher efficiency (0.0925% vs. 0.0083%) with respect to the simple ligand alone. In addition, the J_{SC} and the V_{OC} values were much higher for compound **9** than for NBB. This study demonstrated that commercial dyes can be strongly improved simply by coordinating them to the proper transition metal cation.

In 2022, Kumar et al. [25] synthesized and tested two novel ferrocene sensitizers with an extended π-conjugated system. Dyes **10a–b** consisted of a ferrocene and a phenyl ring separated via an azine spacer. They were different thanks to the hydroxyl group in compound **10a** and the nitro group in **10b** (see Figure 5).

The absorption spectra of **10a** and **10b** were characterized by two bands in the UV region (230 and 326 nm) and by one, less intense, at 474 nm for compound **10a** and at 506 nm for **10b**. The HOMO and LUMO determination of **10a** (+1.04 and −1.42 V) and **10b** (+1.03 and −1.53 V) was necessary and demonstrated the feasibility of electron injection in the TiO_2 conduction band. Even the I^-/I_3^- redox couple was suitable for an efficient dye regeneration.

Compounds **10a–b** and the reference dye **N719** were employed as sensitizers in the DSSCs using a TiO_2 semiconductor and under AM 1.5G conditions. Compound **10a** showed better performances than **10b** and this was attributed to the presence of a hydroxyl group instead of a nitro group (data in Table 2, entries 36–38). The former, in fact,

had a stronger anchoring group than the latter, allowing for a stronger interaction between the dye and the titania layer. This was also demonstrated through the determination of the dye loading, which was 3.89×10^{-7} in the case of **10a** and 3.89×10^{-7} in the case of **10b**. Compound **10a** also presented a longer electron lifetime than **10b** (6.64 vs. 5.82 ns), indicating a delayed recombination of the injected electron with the redox mediator, and hence the higher efficiency of the cell. The presented dyes not only showed very interesting conversion efficiencies but also high efficiencies relative to the reference **N719** (93.04 and 63.92%). Thus, **10a** in particular could be a promising candidate for applications in DSSCs and represents a valid alternative to **N719**.

2.2. Iron Bimetallic Complexes

In the previous subsection, several iron complexes were described as sensitizers for DSSCs. In the meantime, some research groups synthesized and tested bimetallic complexes containing Fe(II) and other cheap and abundant metals, trying to improve the photovoltaic performances.

In 2021, Therien et al. [26] published the new dye **11** consisting of a bimetallic complex of both Fe(II) and Zn(II) (structure in Figure 6). The compound was characterized by two NHC ligands chelating the Fe(II) cation: the first being a simple 2,6-bis(3-methyl-1*H*-3λ^4-imidazol-1-yl)pyridine, and the other the same ligand but functionalized with a zinc porphyrin.
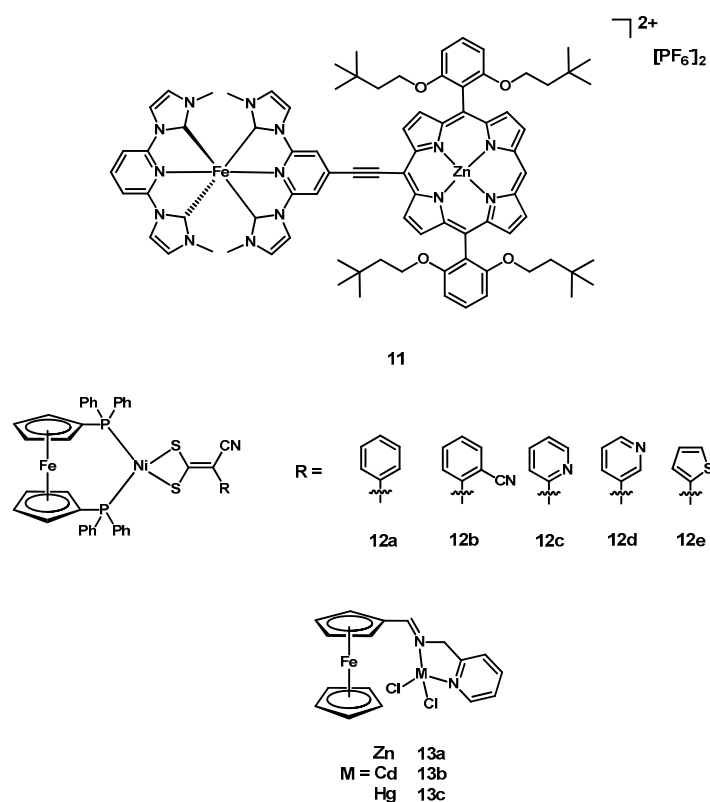
Figure 6. Structure of dyes **11**, **12a–e,** and **13a–c**.

The UV–Vis spectrum of ACN showed a strong absorption band between 400 and 450 nm, with a molar extinction coefficient exceeding 10^5 M^{-1} cm^{-1}, and a weaker band between 600 and 650 nm. From the potentiometric characterization it emerged that the redox potentials of **11** were −1.15 V for the zinc porphyrin and +0.76 V for the couple Fe(II)/Fe(III).

A DSSC fabricated with **11** was compared with another one based on the Ru bipyridine dye **N3**, using TiO₂ on FTO as semiconductor, Pt as counter electrode, and under AM

1.5G irradiation conditions. Only the Jsc and the Voc were determined, and those of **N3** were superior to those of **11** (data in Table 3, entries 1–2). However, the broad intense absorption bands represent a peculiar characteristic of this novel Fe–Zn dye and an important starting point for developing a better performing sensitizer for DSSCs.

Table 3. Photovoltaic data of DSSCs produced with dyes **11**, **12a–e**, and **13a–c** [1].

Entry	Dye	Redox Couple	Jsc (mA cm^{-2})	Voc (V)	FF	η (%)	η$_{rel}$ (%)	Ref.
1	**11** [2,3]	I$^-$/I$_3^-$ [4]	1.25	0.18				[26]
2	**N3** [2,5]	I$^-$/I$_3^-$ [4]	2.10	0.32				[26]
3	**12a**	I$^-$/I$_3^-$	9.39	0.632	0.61	3.61	57.12	[27]
4	**12b**	I$^-$/I$_3^-$	9.93	0.652	0.68	4.39	69.46	[27]
5	**12c**	I$^-$/I$_3^-$	11.25	0.667	0.63	4.76	75.32	[27]
6	**12d**	I$^-$/I$_3^-$	13.15	0.633	0.61	5.05	79.91	[27]
7	**12e**	I$^-$/I$_3^-$	7.94	0.666	0.64	3.36	53.16	[27]
8	**N719**	I$^-$/I$_3^-$	16.44	0.638	0.60	6.32		[27]
9	**13a** [6]	I$^-$/I$_3^-$ [7]	6.08 ± 0.03	0.684 ± 0.02	0.67 ± 0.02	2.79 ± 0.03	66.43	[28]
10	**13b** [6]	I$^-$/I$_3^-$ [7]	5.13 ± 0.04	0.664 ± 0.02	0.67 ± 0.01	2.30 ± 0.04	54.76	[28]
11	**13c** [6]	I$^-$/I$_3^-$ [7]	4.44 ± 0.03	0.656 ± 0.03	0.66 ± 0.01	1.95 ± 0.03	46.43	[28]
12	**13a/N719** [8]	I$^-$/I$_3^-$ [7]	11.25 ± 0.06	0.776 ± 0.02	0.65 ± 0.02	5.71 ± 0.04	135.95	[28]
13	**13b/N719** [8]	I$^-$/I$_3^-$ [7]	10.15 ± 0.04	0.758 ± 0.03	0.65 ± 0.01	5.00 ± 0.05	119.05	[28]
14	**13c/N719** [8]	I$^-$/I$_3^-$ [7]	9.38 ± 0.06	0.742 ± 0.02	0.66 ± 0.01	4.57 ± 0.03	108.81	[28]
15	**N719** [9]	I$^-$/I$_3^-$ [7]	8.85 ± 0.07	0.734 ± 0.02	0.64 ± 0.02	4.20 ± 0.05		[28]

[1] using FTO as conductive oxide, TiO_2 as semiconductor, Pt as counter-electrode, and under AM 1.5G-simulated light source (100 mW cm^{-2}) if not differently specified. [2] SnO_2 semiconductor. [3] 0.5 mM dye in EtOH. [4] 0.5 M TBAI + 0.05 M I_2. [5] 0.5 mM dye in EtOH + 1 mM pyridine-4-carboxylic acid. [6] 10^{-5} M dye in DCM:ACN 1:1. [7] 0.05 M LiI + 0.05 M I_2 + 0.5 M 4-*tert*-butylpyridine in ACN. [8] 10^{-5} M dye + 10^{-5} M **N719** in DCM:ACN 1:1. [9] 10^{-5} M **N719** in EtOH.

In 2021, Gosavi and Kumar et al. [27] synthesized five new 1,1'-bis(diphenylphosphino)ferrocene Ni(II) dithiolates **12a–e** (structures in Figure 6). The difference between these dyes lay in the aromatic substituent on the S^S chelating ligand, namely, a phenyl, a 2-cyanophenyl, 2-pyridyl, 3-pyridyl, and 2-thienyl ring. All these complexes contained at least an anchoring cyano group.

The UV–Vis spectra of compounds **12a–e** were characterized by a medium absorption band between 280 and 350 nm and a weaker one in the 450–500 nm region. From cyclic voltammetry experiments it emerged that the HOMO levels ranged from +0.245 to +0.515 V vs. Ag/Ag$^+$ in ACN. These levels were higher than that of the I$^-$/I$_3^-$ couple (+0.15 V vs. Ag/Ag$^+$ in ACN), which could be used for regenerating the dye. The LUMO levels were between −2.56 and −2.47 V vs. Ag/Ag$^+$ in ACN, indicating a feasible electron injection in the titania film, whose conduction band is placed at +0.75 V vs. Ag/Ag$^+$ in ACN.

Six DSSCs were produced with the five dyes and the reference **N719** using a titania semiconductor film, the I$^-$/I$_3^-$ redox couple, a Pt counter electrode, and under AM 1.5G illumination conditions (data in Table 3, entries 3–8). Despite the higher Jsc and efficiency of **N719**, compound **12d** showed really interesting performances and an 80% relative efficiency with respect to **N719**. Anyway, even compound **12c**, which was an isomer of **12d** due to its differently linked pyridine ring, showed interesting performances. Complexes **12c** and **12d** were also characterized by a longer electron lifetime (5.46 and 6.54 ms, respectively) than **12a**, **12c,** and **12e** (3.26, 4.63, and 2.88 ms), indicating a delayed recombination of the injected electron with the electrolyte, and hence an increased performance. Although these dyes still showed a lower efficiency when compared to the reference **N719**, compounds **12c** and **12d** demonstrated the possibility of more closely approaching the efficiency of the current standard even with cheaper and poorer performing metal centers.

In 2022, Kumar, Sharama, and Chauhan et al. [28] presented three new ferrocenyl-2-pyridilimine complexes **13a–c** (see Figure 6). The employed ligand was the same for the three complexes (ferrocenyl-2-pyridylimine) and it was coordinated to Zn(II), Cd(II), and Hg(II).

The UV–Vis spectra were recorded in MeOH and the maximum absorption wavelengths were 490, 465, and 470 nm for **13a–c**, respectively. The HOMO levels were +0.152, + 0.149, and +0.151 V, while the LUMO levels were −2.53, −2.61, and −2.59 V, clearly indicating that the electron injection in the conduction band of TiO_2 was feasible.

Seven DSSCs were assembled and tested using dyes **13a–c** alone, **13a–c** in combination with **N719**, and with **N719** alone. The selected semiconductor and redox couple were TiO_2 and I^-/I_3^-, and the cells were tested under AM 1.5G conditions (data in Table 3, entries 9–15). Considering the devices fabricated with only the synthesized dyes, much smaller J_{SC}, V_{OC}, and efficiencies than those of **N719** were observed. However, when these dyes were employed together with **N719**, evident improvements of all these parameters were observed, reaching relative efficiencies for **N719** up to 135.95%. This was essentially due to the broader absorption spectrum and to the presence of many more molecules adsorbed on the titania surface, which hindered the diffusion of the oxidized electrolyte towards the photoanode, thereby reducing the recombination of the electrons with the oxidized dye. In fact, the dye loadings were 6.45×10^{-6}, 4.85×10^{-6}, 3.67×10^{-6}, and 3.12×10^{-6} mol cm^{-2} for **N719** and **13a–c**, respectively. After the sensitization, the values for **N719** plus **13a–c** were $4.69 \times 10^{-6} + 2.91 \times 10^{-6}$, $4.87 \times 10^{-6} + 2.12 \times 10^{-6}$, and $4.98 \times 10^{-6} + 1.56 \times 10^{-6}$ mol cm^{-2} and, also in this case, a higher dye loading was observed for **13a**. The electron lifetimes of the devices fabricated with dyes **13a–c** alone were 4.25, 3.94, and 3.26 ms, respectively, and longer lifetimes (6.37, 5.40, and 4.74 ms) were observed when complexes **13a–c** were employed together with **N719**, indicating a less efficient electron recombination with the oxidized electrolyte. These complexes, especially **13a**, represented an important result in the development of novel sensitizers for DSSCs based on non-noble metals. Moreover, when used in combination with **N719**, the efficiency of the **13a/N719** couple exceeded that of the reference dye alone, and this indicated a major step forward in the development of photovoltaic devices.

3. Copper Dyes

As an alternative to iron complexes, several copper complexes have also been tested and published since 2010 [29]. In this subsection, the most recent studies describing the applications of copper complexes in photovoltaic devices are presented. Copper dyes have also been tested employing both the traditional iodine-based redox shuttles and alternative mediators based on copper complexes (an extensive overview on such Cu electrolytes has been published in [30,31]).

In 2018, Housecroft et al. [32] synthesized and tested four novel heteroleptic Cu complexes in DSSCs (**14a–d**, structures in Figure 7). Each ligand had the same core, namely, a simple bipyridine, and they were differentiated by inserting a variety of substituents. The anchoring ligand presented phosphonyl groups for binding to TiO_2. The UV–Vis spectra of complexes **14a–d** were characterized by three separate absorption bands: the first ones were around 280 nm and showed the highest molar absorption coefficients (68,300, 62,500, 73,900, and 69,400 M^{-1} cm^{-1} for complexes **14a–d**). The second ones were around 320 nm and were less intense than those mentioned above (37,400, 44,300, 49,000, and 51,600 M^{-1} cm^{-1} for complexes **14a–d**), while the last values fell between 482 and 486 nm and were much less intense (11,400, 11,400, 13,600, and 13,100 M^{-1} cm^{-1} for complexes **14a–d**). DFT calculations allowed for the examination of the molecular orbitals and, in any case, the LUMO was localized on the anchoring ligand. Four DSSCs, employing dyes **14a–d** and three reference cells with **N719,** were assembled and tested, both on the day in which they were fabricated and after one week. Instead of synthesizing dyes **14a–d** before depositing them onto the TiO_2 layer, the "Surfaces-As-Ligands, Surfaces As Complexes" (SALSAC) method was employed. First, the TiO_2-coated FTO was immersed for 24 h in a solution of a homoleptic Cu(I) complex of the anchoring ligand. After washing the layer with DMSO and EtOH, it was immersed into a DCM solution of a Cu(I) homoleptic complex synthesized with the other ligands, followed by another washing step with EtOH. The DSSC

performances (see Table 4, entries 1–24) showed that compound **14d** was the best Cu sensitizer among the ones considered for this study, followed by **14a** and **14b**. Despite the presence of two methoxy groups on each phenyl ring, compound **14c** was the least interesting sensitizer because the substitution in positions 3 and 5 favored the electron-withdrawing inductive effect, rather than favoring the electron-donating mesomeric effect. After one week, the devices showed only slightly reduced performances, and this clearly indicated a remarkable stability over time. Despite the lower efficiencies when compared to **N719,** compounds **14a–d** are interesting candidates for DSSCs because of their stability over time. Moreover, the SALSAC approach represented a useful tool for the sensitization of the titania film and for its decoration with many different complexes starting from the same anchoring ligand.
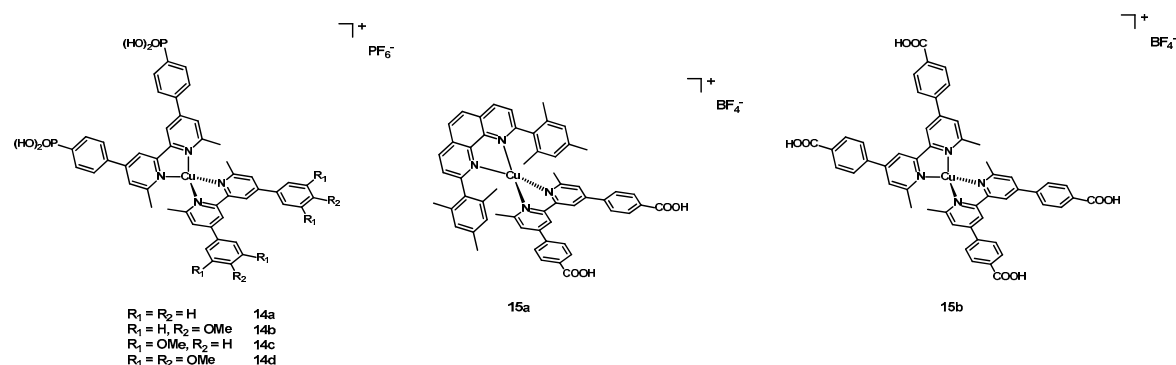

R₁ = R₂ = H **14a**
R₁ = H, R₂ = OMe **14b**
R₁ = OMe, R₂ = H **14c**
R₁ = R₂ = OMe **14d**

Figure 7. Structure of dyes **14a–d** and **15a–b**.

Table 4. Photovoltaic data of DSSCs produced with dyes **14a–d**, **15a–b**, **16a–d**, **17**, and **18a–d** [1].

Entry	Dye	Redox Couple	J_{SC} (mA cm⁻²)	V_{OC} (V)	FF	η (%)	η$_{rel}$ (%)	Ref.
1	**14a** [2,3]	I⁻/I₃⁻ [4]	4.27	0.545	0.71	1.66	28.67	[32]
2	**14a** [2,3]	I⁻/I₃⁻ [4]	4.20	0.536	0.70	1.58	27.29	[32]
3	**N719** (cell 1) [2,3]	I⁻/I₃⁻ [4]	13.29	0.647	0.67	5.79		[32]
4	**14b** [2,3]	I⁻/I₃⁻ [4]	4.87	0.528	0.71	1.82	30.13	[32]
5	**14b** [2,3]	I⁻/I₃⁻ [4]	4.74	0.524	0.72	1.80	29.80	[32]
6	**N719** (cell 2) [2,3]	I⁻/I₃⁻ [4]	13.91	0.635	0.68	6.04		[32]
7	**14c** [2,3]	I⁻/I₃⁻ [4]	3.68	0.528	0.73	1.43	25.44	[32]
8	**14c** [2,3]	I⁻/I₃⁻ [4]	3.90	0.516	0.72	1.46	25.98	[32]
9	**N719** (cell 3) [2,3]	I⁻/I₃⁻ [4]	13.42	0.631	0.66	5.62		[32]
10	**14d** [2,3]	I⁻/I₃⁻ [4]	4.79	0.567	0.72	1.96	33.85	[32]
11	**14d** [2,3]	I⁻/I₃⁻ [4]	4.68	0.550	0.68	1.75	30.22	[32]
12	**N719** (cell 1) [2,3]	I⁻/I₃⁻ [4]	13.29	0.647	0.67	5.79		[32]
13	**14a** [3,5]	I⁻/I₃⁻ [4]	4.22	0.580	0.70	1.72	29.66	[32]
14	**14a** [3,5]	I⁻/I₃⁻ [4]	4.19	0.573	0.70	1.68	28.97	[32]
15	**N719** (cell 1) [3,5]	I⁻/I₃⁻ [4]	12.70	0.670	0.68	5.80		[32]
16	**14b** [3,5]	I⁻/I₃⁻ [4]	4.33	0.569	0.71	1.74	28.02	[32]
17	**14b** [3,5]	I⁻/I₃⁻ [4]	5.02	0.565	0.65	1.86	29.95	[32]
18	**N719** (cell 2) [3,5]	I⁻/I₃⁻ [4]	13.23	0.690	0.68	6.21		[32]
19	**14c** [3,5]	I⁻/I₃⁻ [4]	3.23	0.541	0.74	1.29	21.83	[32]
20	**14c** [3,5]	I⁻/I₃⁻ [4]	4.30	0.562	0.70	1.70	28.76	[32]
21	**N719** (cell 1) [3,5]	I⁻/I₃⁻ [4]	13.05	0.673	0.67	5.91		[32]
22	**14d** [3,5]	I⁻/I₃⁻ [4]	4.75	0.580	0.67	1.86	32.07	[32]
23	**14d** [3,5]	I⁻/I₃⁻ [4]	4.64	0.593	0.65	1.80	31.03	[32]
24	**N719** (cell 3) [3,5]	I⁻/I₃⁻ [4]	12.70	0.670	0.68	5.80		[32]
25	**15a** [6,7]	I⁻/I₃⁻ [8]	9.00	0.61	0.63	3.50	39.33	[31]
26	**15a** [6,7]	I⁻/I₃⁻ [9]	8.20	0.67	0.65	3.60	40.45	[31]
27	**15a** [6,7]	Cu⁺/Cu²⁺ [10]	4.70	0.75	0.36	1.30	14.61	[31]
28	**15a** [6,7]	Cu⁺/Cu²⁺ [11]	6.30	0.61	0.53	2.00	22.47	[31]
29	**15b** [6,7]	I⁻/I₃⁻ [8]	7.30	0.59	0.69	3.00	33.71	[31]
30	**N719** [6,7]	I⁻/I₃⁻ [8]	15.40	0.80	0.71	8.90		[31]
31	**16a** [3]	Cu⁺/Cu²⁺ [12]	1.10	0.558	0.55	0.33	6.11	[33]

32	**16b** [3]	Cu^+/Cu^{2+} [13]	1.69	0.662	0.55	0.61	11.30	[33]
33	**16c** [3]	Cu^+/Cu^{2+} [13]	1.97	0.648	0.43	0.54	10.00	[33]
34	**16d** [3]	Cu^+/Cu^{2+} [13]	1.88	0.655	0.52	0.64	11.85	[33]
35	**16a** [3]	Cu^+/Cu^{2+} [14]	2.14	0.784	0.66	1.12	20.74	[33]
36	**16b** [3]	Cu^+/Cu^{2+} [14]	2.15	0.710	0.55	0.84	15.56	[33]
37	**16c** [3]	Cu^+/Cu^{2+} [14]	2.29	0.689	0.60	0.95	17.59	[33]
38	**16d** [3]	Cu^+/Cu^{2+} [14]	2.21	0.679	0.64	0.97	17.96	[33]
39	**16e** [3]	Cu^+/Cu^{2+} [14]	2.27	0.702	0.61	0.97	17.96	[33]
40	**16b** [3]	Cu^+/Cu^{2+} [15]	3.09	0.812	0.72	1.82	33.70	[33]
41	**16c** [3]	Cu^+/Cu^{2+} [15]	2.80	0.796	0.73	1.63	30.19	[33]
42	**16d** [3]	Cu^+/Cu^{2+} [15]	2.98	0.804	0.74	1.76	32.59	[33]
43	**16e** [3]	Cu^+/Cu^{2+} [15]	2.66	0.788	0.73	1.53	28.33	[33]
44	**16c** [3]	Cu^+/Cu^{2+} [16]	3.85	0.686	0.76	2.00	37.04	[33]
45	**16d** [3]	Cu^+/Cu^{2+} [16]	3.44	0.681	0.75	1.76	32.59	[33]
46	**16e** [3]	Cu^+/Cu^{2+} [16]	4.01	0.684	0.75	2.06	38.15	[33]
47	**N719** [17]	I^-/I_3^-	12.54	0.614	0.70	5.40		[33]
48	**17** [2,18]	I^-/I_3^- [4]	4.36	0.517	0.690	1.55	22.66	[34]
49	**17** [2,18]	I^-/I_3^- [4]	4.88	0.528	0.701	1.80	26.32	[34]
50	**17** [2,19]	I^-/I_3^- [4]	5.95	0.560	0.682	2.27	33.19	[34]
51	**17** [2,19]	I^-/I_3^- [4]	6.17	0.550	0.673	2.29	33.48	[34]
52	**17** [2,20]	I^-/I_3^- [4]	7.85	0.524	0.683	2.81	41.08	[34]
53	**17** [2,20]	I^-/I_3^- [4]	7.73	0.517	0.678	2.71	39.62	[34]
54	**N719** [2,17]	I^-/I_3^- [4]	15.33	0.615	0.726	6.84		[34]
55	**17** [18,21]	I^-/I_3^- [4]	2.63	0.499	0.678	0.89	12.18	[34]
56	**17** [19,21]	I^-/I_3^- [4]	3.45	0.514	0.694	1.23	16.83	[34]
57	**17** [19,21]	I^-/I_3^- [4]	5.69	0.560	0.694	2.21	30.23	[34]
58	**17** [20,21]	I^-/I_3^- [4]	6.38	0.560	0.689	2.46	33.65	[34]
59	**17** [20,21]	I^-/I_3^- [4]	6.58	0.515	0.714	2.42	33.11	[34]
60	**17** [20,21]	I^-/I_3^- [4]	7.77	0.545	0.637	2.69	36.80	[34]
61	**N719** [17,21]	I^-/I_3^- [4]	15.73	0.638	0.729	7.31		[34]
62	**17** [5,18]	I^-/I_3^- [4]	2.61	0.501	0.681	0.89	12.08	[34]
63	**17** [5,18]	I^-/I_3^- [4]	3.33	0.505	0.690	1.16	15.74	[34]
64	**17** [5,19]	I^-/I_3^- [4]	5.60	0.561	0.706	2.22	30.12	[34]
65	**17** [5,19]	I^-/I_3^- [4]	6.18	0.560	0.702	2.43	32.97	[34]
66	**17** [5,20]	I^-/I_3^- [4]	7.13	0.535	0.694	2.65	35.96	[34]
67	**17** [5,20]	I^-/I_3^- [4]	8.10	0.561	0.576	2.61	35.41	[34]
68	**N719** [5,17]	I^-/I_3^- [4]	15.16	0.672	0.724	7.37		[34]
69	**16a** [3]	I^-/I_3^- [4]	4.61	0.521	0.72	1.72	27.52	[35]
70	**16a** [3,22]	I^-/I_3^- [4]	5.11	0.535	0.72	1.97	31.52	[35]
71	**16a** [3,23]	I^-/I_3^- [4]	4.59	0.512	0.70	1.65	26.40	[35]
72	**16a** [3,24]	I^-/I_3^- [4]	2.11	0.434	0.69	0.63	10.08	[35]
73	**16a** [3,25]	I^-/I_3^- [4]	0.75	0.404	0.70	0.21	3.36	[35]
74	**N719** [17]	I^-/I_3^- [4]	14.30	0.635	0.70	6.25		[35]
75	**18a** [26]	I^-/I_3^- [27]	9.35	0.67	0.663	4.17		[36]
76	**18b** [26]	I^-/I_3^- [27]	9.02	0.65	0.652	3.82		[36]
77	**18c** [26]	I^-/I_3^- [27]	12.54	0.75	0.696	6.55		[36]
78	**18d** [26]	I^-/I_3^- [27]	12.06	0.72	0.684	6.06		[36]

[1] using FTO as conductive oxide, TiO_2 as semiconductor, Pt as counter-electrode, and under AM 1.5 G-simulated light source (100 mW cm^{-2}) if not differently specified. [2] tested on the day of DSSC fabrication. [3] 1.0 M anchoring ligand in DMSO; then, 0.1 M homoleptic complex with ancillary ligands in DCM. [4] 0.1 M LiI + 0.05 M I_2 + 0.5 M 1-methylbenzimidazole + 0.6 M 1-butyl-3-methylimidazolium iodide (BMII) in MPN. [5] tested seven days after the DSSC fabrication. [6] Use of an Abet 2000 solar simulator with a 300 W xenon lamp adjusted with a calibrated solar cell (VLSI standard SRC-1000-RTD-KG5). [7] 1.5×10^{-3} M in MeOH. [8] 0.025 M LiI + 0.04 M I_2 + 0.65 M BMII in ACN + 0.28 M TBP in 15:85 valeronitrile (BuCN)/ACN. [9] 0.01 M LiI + 0.017 M I_2 + 0.26 M BMII in ACN + 0.28 M TBP in 15:85 BuCN/ACN. [10] 0.17 M **E1** + 0.017 M **E2** + 0.1 M LiTFSI (LiTFSI = Lithium bis(trifluoromethanesulfonyl)imide) in ACN. [11] 0.17 M **E3** + 0.014 M **E4** + 0.1 M LiTFSI in ACN. [12] **E5/E6** 5:1 + TBP + LiPF$_6$ in ACN. [13] **E7/E8** + TBP + LiPF$_6$ in ACN. [14] **E9/E10** + TBP + LiPF$_6$ in ACN. [15] **E11/E12** + TBP + LiPF$_6$ in ACN. [16] **E13/E14** + TBP + LiPF$_6$ in ACN. [17] 0.3 mM **N719** in EtOH. [18] ligand exchange dipping procedure. [19] 1:1 dipping procedure. [20] sequential procedure. [21] tested three days after the DSSC fabrication. [22] 1 eq. TBAOH respect to the anchoring ligand. [23] 2 eq. TBAOH respect to the anchoring ligand. [24] 3 eq. TBAOH respect to the anchoring ligand. [25] 4 eq. TBAOH respect to

the anchoring ligand. [26] 0.5 mM dye in *N*,*N*-dimethylformamide (DMF). [27] 0.5 M LiI + 0.05 M I$_2$ + 0.5 M TBP in ACN:MPN 7:3 *v/v*.

In 2018, Colombo et al. [31] synthesized two new Cu-phenanthroline complexes for applications in DSSCs. In particular, compounds **15a–b** (structures in Figure 7) were functionalized with two anchoring carboxylic groups and employed as sensitizers, whereas homoleptic compounds **E1–4** (see Figure 8), in which the ligands were much simpler than those of **15a–b**, were employed as redoxelectrolytic couples.
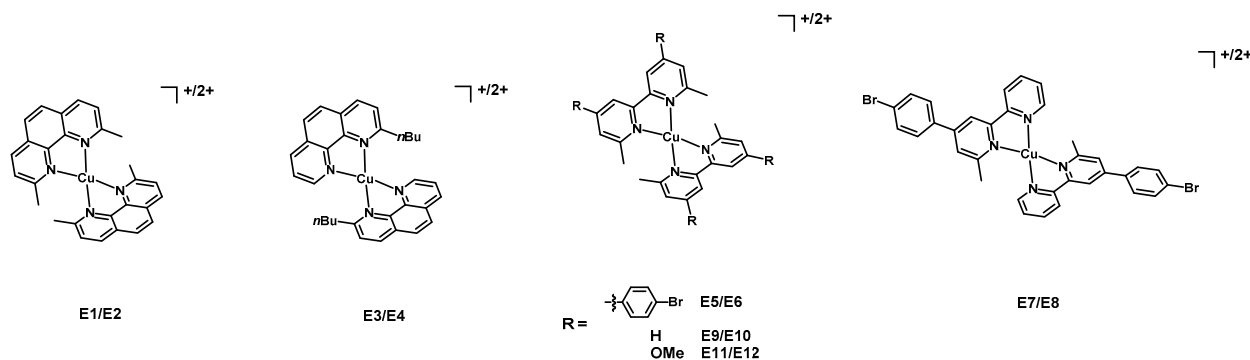
Figure 8. Structure of redox couples **E1–E12**. In all cases, the counteranions are PF$_6^-$.

The UV–Vis spectra of **15a** and **E1–4** had a broad and intense band around 460 nm when the oxidation state of the metal center was +1, and a significant red shift to around 750 nm and a decrease in the molar absorption coefficient were observed in the case of the Cu(II) complexes (**15a**: λ_{max} = 478 nm, ε = 7.6 × 10^3 M^{-1} cm^{-1}, **E1**: λ_{max} = 455 nm, ε = 8.0 × 10^3 M^{-1} cm^{-1}, **E2**: λ_{max} = 741 nm, ε = 2.3 × 10^4 M^{-1} cm^{-1}, **E3**: λ_{max} = 452 nm, ε = 6.2 × 10^3 M^{-1} cm^{-1}, **E4**: λ_{max} = 756 nm, ε = 9.6 × 10^5 M^{-1} cm^{-1}). Cyclic voltammetry experiments demonstrated that both the **E1**/**E2** and **E3**/**E4** couples were capable of restoring the oxidized dyes, but a better performance was observed in the case of the heteroleptic complex **15a**.

Dyes **15a–b** were employed as sensitizers in DSSCs and compared with the reference **N719** (data in Table 4, entries 25–30). The chosen redox electrolytes were the classical I$^-$/I$_3^-$ couple and the novel couples **E1**/**E2** and **E3**/**E4** with the aim of making cheaper and environmentally friendly full-copper DSSCs. A higher efficiency was observed when the I$^-$/I$_3^-$ was used, due to different reasons: first, the Cu-based electrolytes were able to absorb light thanks to their broad absorption bands and high molar extinction coefficients. Second, their solubilities were much lower than those of the components of the I$^-$/I$_3^-$ couple and working with a 2.4-fold further diluted solution resulted in a much lower efficiency. Although complexes **15a–b** were much more underperforming than **N719** and even though the use of Cu-based redox mediators decreased the photovoltaic performances even more, this article demonstrated the feasibility of full-copper DSSCs. Moreover, the Cu(I)/Cu(II) redox couples were not corrosive, in contrast to the I$^-$/I$_3^-$ couple, so their optimization (especially of the better performing **E3**/**E4**) will lead to higher efficiencies.

In 2018, Housecroft et al. [33] presented an example of a full-copper DSSC, with a heteroleptic Cu(I) complex as a sensitizer and a redox couple consisting of Cu$^{+/2+}$ homoleptic compounds. Concerning the dyes, the anchoring ligand was in all cases a 4,4'-di(4-PO(OH)$_2$-phenyl)-6,6'dimethylbipyridine, while the ancillary ligands were differently substituted bipyridines or a phenanthroline (**16a–e**, see Figure 9). These ancillary N^N ligands were also used for the synthesis of four novel homoleptic complexes (**E5–E12**, Figure 8) tested as electrolytes and compared to **E1**/**E2**, with whom a total of sixteen devices were fabricated.
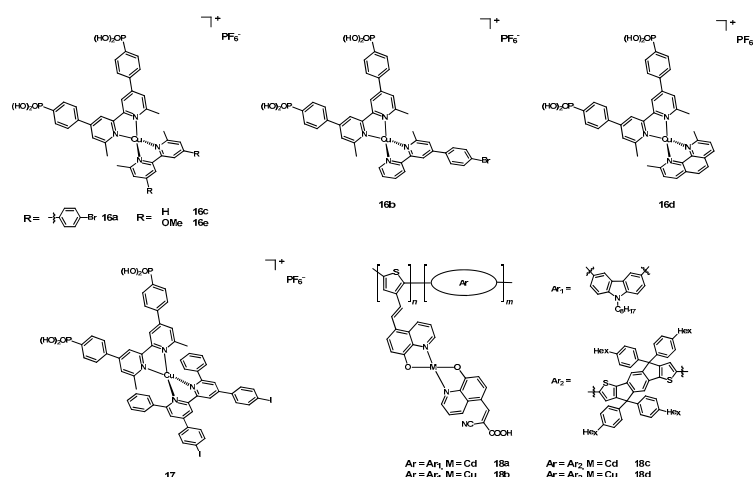
Figure 9. Structure of dyes **16a–e**, **17,** and **18a–d**.

The lowest efficiency (0.33%) was observed by combining **16a** and **E5/E6**, which provided a Jsc of 1.10 mA cm^{-2}, which was probably due to the poor solubility of **E5/E6** in ACN. The use of **16b** with **E7/E8** lead to a Voc value higher than that of the reference cell with the standard dye **N719** (662 vs. 614 mV). Moreover, the best-performing devices were those based on **16b–d** and having **E11/E12** as an electrolyte, showing high values of Jsc (in the range 3.44–4.01 mA cm^{-2}) and an FF around 75%.

The highest efficiency with respect to reference **N719** (2.06%, representing a η_{rel} of 38.1%) was achieved by testing **16e** in combination with **E11/E12**. The complete data are reported in Table 4, entries 31–47.

In 2018, Constable et al. [34] synthesized and tested the heteroleptic dye **17** (structure in Figure 9). Similar to complexes **14a–d**, the ligands were constituted by a 2,2′-bipyridine functionalized with different groups. In addition, in this case, the anchoring ligand contained phosphonyl groups and the dye was assembled through the SALSAC approach starting from the functionalization of the TiO$_2$ layer with the anchoring ligand.

The UV–Vis spectrum of **17** in DCM was characterized by an intense band around 325 nm and two much less intense ones at 435 and 485 nm.

Six DSSCs were produced using complex **17** as a sensitizer and through the ligand-exchange method, the 1:1 dipping procedure, and by sequential assembly (each method was employed to make two cells) and compared with a cell fabricated with **N719** (see Table 4, entries 48–68). The three different dipping procedures differed in the way in which the non-anchoring ligand was coordinated to the metal center. The titania film was firstly functionalized with the anchoring ligand by immersing the electrode in a 1.0 mM solution in DMSO and washing it with DMSO and EtOH. After that, the ligand exchange method included its immersion into a DCM solution of the homoleptic Cu complex containing the non-anchoring ligand. In the case of the 1:1 method, the electrode was immersed into a 0.1 mM solution of [Cu(CH$_3$CN)$_4$][PF$_6$] and in a 0.1 mM solution of the non-anchoring ligand in DCM. On the other hand, the sequential method started with the immersion of the electrode into a 2.0 mM solution of [Cu(CH$_3$CN)$_4$][PF$_6$] in can followed by the immersion of the same electrode in a 0.1 mM solution of the non-anchoring ligand in DCM. In any case, the solid-state UV–Vis spectra of each cell showed the presence of both the homoleptic complex containing two anchoring ligands and dye **17**. The best-performing cells were those fabricated through the sequential method, with a Jsc around 7.8 mA cm^{-2} and an efficiency of 2.8%. The lowest performances were observed with the DSSCs fabricated through the ligand-exchange protocol. Even if the relative efficiencies of the cells fabricated with complex **17** were lower than that of the reference cell with **N719** (the highest relative efficiency was 41.1%), and despite the existence of a minimum degradation of the photovoltaic performances over time, this article compared three different dipping protocols and demonstrated that the best one was the sequential method. Therefore,

its optimization, together with the synthesis of optimized ligands, will further improve the performances of such cells.

In the same year, Housecroft and coworkers [35] carried out a study on the effect of the partial deprotonation of the aforementioned anchoring ligand based on a 4,4′-di(4-PO(OH)$_2$-phenyl)-6,6′dimethylbipyridine (**16a**, Figure 9). The deprotonation was achieved by the subsequent addition of different equivalents of bases (tetrabutylammonium hydroxide (TBAOH), NaOH, Cs$_2$CO$_3$) to DMSO solutions of the complex, monitoring the effect through ^{1}H and ^{31}P NMR spectroscopy.

After the addition of 1 eq. of the base, an important increase in the efficiency (as a consequence of the higher Voc and Jsc) was observed; this phenomenon, with an increase up to 26%, was explained by an enhanced solubility of the deprotonated species, causing a more efficient binding of the dye molecules on the TiO$_2$ surface and leading to better electron transfer.

The addition of further equivalents of the base resulted in a decrease in the efficiency accompanied by the appearance of a precipitate, limiting the solubility of the dye (see Table 4, entries 69–74).

In 2018, Zhong et al. [36] synthesized four new polymeric metal complexes **18a–d** (structures in Figure 9) containing Cu and Cd metal centers. The dyes were constituted by a donor (D) and an acceptor (A) connected through a conjugated π-bridge with an additional acceptor to obtain a D-A-π-A structure. In this way, it was possible to minimize the intramolecular charge recombination between the donor and acceptor. In this study, the donors were the electron-rich indacenodithiophene and carbazole, the anchoring acceptor was cyanoacrylic acid, while the additional acceptor was a Cu or Cd complex with two 8-hydroxyquinoline ligands.

The UV–Vis spectra of the carbazole-based complexes **18a–b** were characterized by an absorption maximum at 439 or at 416 nm depending on the metal center, Cd or Cu, respectively, with 24,400 and 24,100 M^{-1} cm^{-1} molar extinction coefficients. Remarkably red-shifted absorption bands (531 and 508 nm for the Cd and the Cu dyes) with slightly higher molar extinction coefficients (25,500 and 25,000 M^{-1} cm^{-1}) were observed when the donor was indacenodithiophene, being a stronger donor than carbazole. The smaller red shift observed when passing from Cu to Cd was attributed to the larger radius of Cd, which improved the π-back donation between the ligands and the metal center. The electrochemical characterization of **18a–d** showed that the HOMO levels fell between −5.32 and −5.46 eV, while the LUMO levels were between −3.00 and −3.45 eV. This indicated the possibility of dye restoration by the I$^-$/I$_3^-$ redox couple (−4.83 eV) and an efficient electron injection in the titania film (−4.26 eV). The polymers were also subject to a Thermal Gravimetric Analysis (TGA) under a N$_2$ atmosphere: each dye showed an excellent stability and the onset temperature, at which 5% loss took place, was higher than 300 °C. This demonstrated that these polymers were very stable and that they could be used as sensitizers in DSSCs.

The photovoltaic parameters—listed in Table 4, entries 75–78—demonstrated the superior performances of the indacenodithiophene-based dyes due to its higher planarity than carbazole. Cd, thanks to its stronger electron-withdrawing character with respect to Cu, guaranteed only slightly higher performances; nevertheless, an interesting conversion efficiency was reached even with the Cu-indacenodithiophene dye. The optimization of this dye could lead to the discovery of Cu complexes with even better performances.

In 2019, Dragonetti et al. [37] optimized the performances of full-copper DSSCs fabricated with the abovementioned dye, **15a**, working on an electrolyte solution based on the **E3/E4** redox couple. For a more detailed comparison, the classical I$^-$/I$_3^-$ redox couple and a control cell employing **N719** were also tested.

The photovoltaic performances (see Table 5, entries 1–10) were remarkable for the cell containing a simple dye such as **15a** and the I$^-$/I$_3^-$ redox couple (η = 3.05%); and were better than those of the full-copper cells because of the much higher electrolyte concentration. An important enhancement of the performances of full-copper DSSCs was observed

by employing a more diluted solution of **E3/E4** in the presence of LiTFSI, since even the electrolyte was able to absorb sunlight, and a lower concentration of **E3/E4** reduced these absorption phenomena. On the other hand, the highest efficiency for a full-copper DSSC was obtained without diluting the redox electrolyte and by introducing both LiTFSI and TBP. The latter had a higher affinity for Cu(II) rather than Cu(I), and the penta-coordinated species exhibited higher recombination energies, which resulted in a slower charge recombination process. This work clearly explained the feasibility of full-copper DSSCs and the possibility of enhancing their performances through the electrolyte.

Table 5. Photovoltaic data of DSSCs produced with dyes **15a**, **19a–b**, **20a–e**, **21a–c**, **22a–c**, **23a–d**, **24a–e**, and **25a–d** [1].

Entry	Dye	Redox Couple	J_{SC} (mA cm^{-2})	V_{OC} (V)	FF	η (%)	η_{rel} (%)	Ref.
1	**15a** [2,3]	I$^-$/I$_3^-$ [4]	6.17	0.670	0.739	3.05	44.40	[37]
2	**15a** [2,3]	I$^-$/I$_3^-$ [5]	6.41	0.648	0.730	3.03	44.10	[37]
3	**15a** [2,3]	Cu$^+$/Cu^{2+} [6]	4.06	0.606	0.639	1.57	22.85	[37]
4	**15a** [2,3]	Cu$^+$/Cu^{2+} [7]	3.69	0.708	0.627	1.64	23.87	[37]
5	**15a** [2,3]	Cu$^+$/Cu^{2+} [8]	4.35	0.630	0.631	1.73	25.18	[37]
6	**15a** [2,3]	Cu$^+$/Cu^{2+} [9]	2.88	0.725	0.599	1.25	18.20	[37]
7	**15a** [2,3]	Cu$^+$/Cu^{2+} [10]	5.77	0.622	0.701	2.51	36.54	[37]
8	**15a** [2,3]	Cu$^+$/Cu^{2+} [11]	4.98	0.543	0.662	1.84	26.78	[37]
9	**15a** [2,3]	Cu$^+$/Cu^{2+} [12]	2.22	0.705	0.560	0.88	12.81	[37]
10	**N719** [2,3]	I$^-$/I$_3^-$ [13]	15.17	0.659	0.687	6.87		[37]
11	**15a** [2,3]	I$^-$/I$_3^-$ [14]	6.10	0.592	0.710	2.50	28.09	[38]
12	**15a** [2,3]	I$^-$/I$_3^-$ [15]	4.70	0.571	0.740	2.00	22.47	[38]
13	**19a** [2,3]	I$^-$/I$_3^-$ [14]	5.60	0.602	0.750	2.50	28.09	[38]
14	**19a** [2,3]	I$^-$/I$_3^-$ [15]	5.20	0.607	0.750	2.30	25.84	[38]
15	**19b** [2,3]	I$^-$/I$_3^-$ [14]	5.80	0.597	0.740	2.60	29.21	[38]
16	**19b** [2,3]	I$^-$/I$_3^-$ [15]	5.60	0.599	0.720	2.40	26.97	[38]
17	**15a** [2,3]	Cu$^+$/Cu^{2+} [16]	2.90	0.694	0.360	0.70	7.87	[38]
18	**19a** [2,3]	Cu$^+$/Cu^{2+} [16]	2.60	0.647	0.350	0.60	6.74	[38]
19	**19b** [2,3]	Cu$^+$/Cu^{2+} [16]	0.90	0.370	0.370	0.10	1.12	[38]
20	**15a** [2,3]	Cu$^+$/Cu^{2+} [17]	3.80	0.593	0.610	1.40	15.73	[38]
21	**19a** [2,3]	Cu$^+$/Cu^{2+} [17]	3.20	0.570	0.670	1.20	13.48	[38]
22	**19b** [2,3]	Cu$^+$/Cu^{2+} [17]	2.80	0.573	0.620	1.00	11.24	[38]
23	**N719** [2,3]	I$^-$/I$_3^-$ [15]	15.4	0.802	0.71	8.9		[38]
24	**20a**	I$^-$/I$_3^-$ [18]	3.93	0.67	0.69	1.81	35.35	[39]
25	**20b**	I$^-$/I$_3^-$ [18]	6.88	0.63	0.76	3.29	64.26	[39]
26	**20c**	I$^-$/I$_3^-$ [18]	7.49	0.67	0.72	3.62	70.70	[39]
27	**20d**	I$^-$/I$_3^-$ [18]	5.64	0.69	0.73	2.84	55.47	[39]
28	**20e**	I$^-$/I$_3^-$ [18]	2.77	0.68	0.71	1.33	25.98	[39]
29	**N719**	I$^-$/I$_3^-$ [18]	12.90	0.62	0.64	5.12		[39]
30	**21a** [19]	-	5.99	0.56	0.53	1.77		[40]
31	**21b** [19]	-	4.96	0.58	0.52	1.51		[40]
32	**21c** [19]	-	5.48	0.49	0.53	1.43		[40]
33	**22a** [20]	I$^-$/I$_3^-$	5.56	0.64	0.43	1.54		[41]
34	**22b** [20]	I$^-$/I$_3^-$	4.94	0.59	0.46	1.35		[41]
35	**22c** [20]	I$^-$/I$_3^-$	5.20	0.69	0.47	1.69		[41]
36	**23a** [21,22,23,24,25]	I$^-$/I$_3^-$ [26]		0.689		3.77		[42]
37	**23b** [21,22,23,25,27]	I$^-$/I$_3^-$ [26]		0.685		3.80		[42]
38	**23c** [21,22,23,24,25]	I$^-$/I$_3^-$ [26]		0.686		4.32		[42]
39	**23d** [21,22,23,25,27]	I$^-$/I$_3^-$ [26]		0.682		4.36		[42]
40	**24a** [28]	I$^-$/I$_3^-$ [29]	4.08	0.538	0.69	1.51	26.31	[43]
41	**24a** [28]	I$^-$/I$_3^-$ [29]	3.64	0.520	0.69	1.32	23.00	[43]
42	**24a** [28]	I$^-$/I$_3^-$ [29]	3.87	0.534	0.70	1.44	25.09	[43]
43	**24b** [28]	I$^-$/I$_3^-$ [29]	3.40	0.526	0.71	1.28	22.30	[43]
44	**24b** [28]	I$^-$/I$_3^-$ [29]	3.01	0.530	0.72	1.14	19.86	[43]
45	**24b** [28]	I$^-$/I$_3^-$ [29]	3.44	0.524	0.70	1.26	21.95	[43]
46	**24c** [28]	I$^-$/I$_3^-$ [29]	4.08	0.522	0.68	1.45	25.26	[43]
47	**24c** [28]	I$^-$/I$_3^-$ [29]	3.51	0.522	0.70	1.28	22.30	[43]
48	**24c** [28]	I$^-$/I$_3^-$ [29]	3.40	0.518	0.71	1.26	21.95	[43]
49	**24d** [28]	I$^-$/I$_3^-$ [29]	2.83	0.508	0.70	1.01	17.60	[43]

50	**24d** [28]	I⁻/I₃⁻ [29]	2.96	0.516	0.71	1.08	18.82	[43]
51	**24d** [28]	I⁻/I₃⁻ [29]	2.74	0.514	0.70	0.99	17.25	[43]
52	**24e** [28]	I⁻/I₃⁻ [29]	1.56	0.455	0.65	0.46	8.01	[43]
53	**24e** [28]	I⁻/I₃⁻ [29]	1.49	0.461	0.66	0.45	7.84	[43]
54	**24e** [28]	I⁻/I₃⁻ [29]	1.55	0.455	0.65	0.46	8.01	[43]
55	**N719** [30]	I⁻/I₃⁻ [29]	13.42	0.640	0.67	5.74		[43]
56	**25a** [28]	I⁻/I₃⁻ [29]	4.54	0.541	0.676	1.66	30.97	[44]
57	**25a** [28]	I⁻/I₃⁻ [29]	4.69	0.539	0.681	1.72	32.09	[44]
58	**25a** [28]	I⁻/I₃⁻ [29]	4.74	0.539	0.701	1.79	33.40	[44]
59	**25a** [28]	I⁻/I₃⁻ [29]	4.55	0.524	0.697	1.66	30.97	[44]
60	**25a** [28,31]	I⁻/I₃⁻ [29]	4.75	0.534	0.651	1.65	30.78	[44]
61	**25a** [28,31]	I⁻/I₃⁻ [29]	4.75	0.548	0.689	1.79	33.40	[44]
62	**25a** [28,31]	I⁻/I₃⁻ [29]	4.42	0.545	0.659	1.59	29.66	[44]
63	**25a** [28,31]	I⁻/I₃⁻ [29]	4.73	0.543	0.688	1.77	33.02	[44]
64	**25b** [28]	I⁻/I₃⁻ [29]	3.59	0.514	0.707	1.30	24.25	[44]
65	**25b** [28]	I⁻/I₃⁻ [29]	3.64	0.508	0.696	1.29	24.07	[44]
66	**25b** [28]	I⁻/I₃⁻ [29]	3.54	0.513	0.712	1.29	24.07	[44]
67	**25b** [28]	I⁻/I₃⁻ [29]	3.57	0.514	0.684	1.25	23.32	[44]
68	**N719** [30]	I⁻/I₃⁻ [29]	14.13	0.602	0.630	5.36		[44]
69	**25c** [28]	I⁻/I₃⁻ [29]	4.82	0.532	0.679	1.74	33.59	[44]
70	**25c** [28]	I⁻/I₃⁻ [29]	5.25	0.523	0.703	1.93	37.26	[44]
71	**25c** [28]	I⁻/I₃⁻ [29]	4.64	0.536	0.686	1.71	33.01	[44]
72	**25c** [28]	I⁻/I₃⁻ [29]	4.89	0.533	0.668	1.74	33.59	[44]
73	**25d** [28]	I⁻/I₃⁻ [29]	4.24	0.535	0.693	1.57	30.31	[44]
74	**25d** [28]	I⁻/I₃⁻ [29]	3.96	0.530	0.686	1.44	27.80	[44]
75	**25d** [28]	I⁻/I₃⁻ [29]	4.08	0.534	0.668	1.46	28.19	[44]
76	**25d** [28]	I⁻/I₃⁻ [29]	4.05	0.531	0.703	1.51	29.15	[44]
77	**N719** [30]	I⁻/I₃⁻ [29]	14.25	0.603	0.603	5.18		[44]

[1] using FTO as conductive oxide, TiO_2 as semiconductor, Pt as counter-electrode, and under AM 1.5G-simulated light source (100 mW cm⁻²) if not differently specified. [2] Use of an Abet 2000 solar simulator with a 300 W xenon lamp adjusted with a calibrated solar cell (VLSI standard SRC-1000-RTD-KG5). [3] 1.5 mM dye in MeOH. [4] 0.01 M LiI + 0.017 M I₂ + 0.26 M BMII + 0.28 M TBP in 15:85 *v/v* BuCN:ACN. [5] 0.01 M LiI + 0.017 M I₂ + 0.26 M BMII + 0.28 M TBP + 0.025 M guanidinium iodide (GuI) in 15:85 *v/v* BuCN:ACN. [6] 0.085 M **E3** + 0.0085 M **E4** + 0.05 M LiTFSI in ACN. [7] 0.085 M **E3** + 0.0085 M **E4** + 0.14 M TBP + 0.05 M LiTFSI in ACN. [8] 0.038 M **E3** + 0.0038 M **E4** + 0.022 M LiTFSI in ACN. [9] 0.038 M **E3** + 0.0038 M **E4** + 0.062 M TBP + 0.022M LiTFSI in ACN. [10] 0.085 M **E3** + 0.0085 M **E4** + 0.28 M TBP + 0.1 M LiTFSI in ACN. [11] 0.038 M **E3** + 0.0038 M **E4** + 0.28 M TBP + 0.1 M LiTFSI in ACN. [12] 0.085 M **E3** + 0.0085 M **E4** + 0.28 M TBP + 0.1 M LiTFSI + 0.26 M MBIPF₆ ([N-methyl-N-butylimidazolium][PF6]) in ACN. [13] 0.6 M BMII + 0.03 M I2 + 0.1 M GuNCS + 0.5 M TBP in 15:85 *v/v* BuCN:ACN. [14] 0.025 M LiI + 0.04 M I₂ + 0.65 M BMII + 0.28 M TBP in 15:85 BuCN:ACN. [15] 0.025 M LiI + 0.04 M I2 + 0.65 M BMII + 0.05 M GuI + 0.28 M TBP in 15:85 BuCN:ACN. [16] 0.17 M **E1** + 0.017 **E2** + 0.1 M LiTFSI in ACN. [17] 0.17 M **E3** + 0.017 **E4** + 0.1 M LiTFSI in ACN. [18] Solaronix Iodolyte AN-50. [19] Cu₂S was used as counter electrode. [20] 1 mM dye in DMF. [21] Indium tin oxide (ITO) was used as conductive oxide instead of FTO. [22] ITO functionalized with NrGONS was used as counter electrode. [23] Use of an Autolab Potentiostat/Galvanostat 302 N with FRA Module and LED kit to test the photovoltaic performances of the cells. [24] TiO₂ functionalized with rGONS was used as semiconductor. [25] 0.05 mM dye in EtOH. [26] 0.5 M LiI + 0.05 M I₂ in ACN. [27] TiO₂ functionalized with NrGONS was used as semiconductor. [28] 1.0 mM anchoring dye in DMSO, then 0.1 mM homoleptic complex in DCM. [29] 0.1 M LiI + 0.05 M I₂ + 0.5 M 1-methylbenzimidazole + 0.6 M BMII in MPN. [30] 0.3 mM **N719** in EtOH. [31] Use of decylphosphonic acid (DPA) as co-adsorbent.

In 2019, Colombo et al. [38] synthesized two novel heteroleptic Cu complexes **19a–b** (see Figure 10) and compared them with the previously described **15a**. Unlike the simple phenanthroline ligand employed for dye **15a**, more functionalized ones were employed for **19a–b**, one containing a triphenylamine, the other with a 3-hexyloxyphenyl moiety. In addition, in this case, the I⁻/I₃⁻, **E1/E2** and **E3/E4** couples were employed as redox mediators.
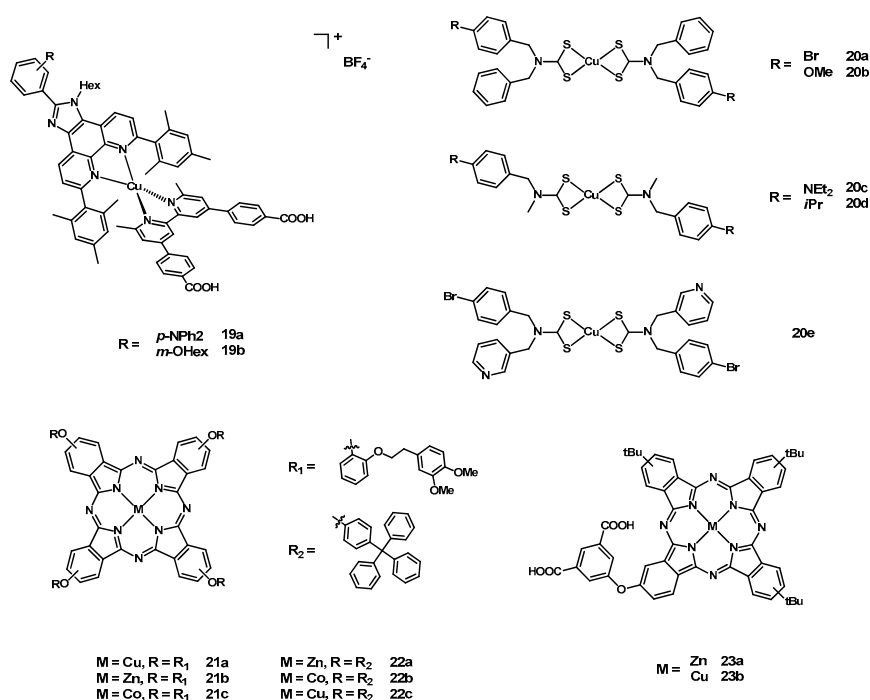
Figure 10. Structure of dyes **19a–b**, **20a–e**, **21a–c**, **22a–c**, and **23a–b**.

The UV–Vis spectra showed that the more extended π-conjugated system of complexes **19a–b** brought about a red shift from 478 to 491 and 490 nm, respectively, and a noticeable increase in the molar absorption coefficients from 7.6×10^3 to 9.3×10^3 and 12.0×10^3 M^{-1} cm^{-1}. DFT calculations demonstrated that the HOMO was mainly localized over the metal center, while the LUMO was localized over the anchoring ligand, which implied an efficient electron injection in the TiO₂ conduction band. Cyclic voltammetry experiments showed that the **E3**/**E4** redox couple was better than **E1**/**E2** thanks to the larger difference between the oxidation potentials of the dye and of the redox mediator (0.28 vs. 0.09 eV).

The performances of solar cells fabricated with the complexes **15**, **19a–b,** and **N719** employing both the I^-/I_3^-, **E1**/**E2,** and **E3**/**E4** redox couples (summarized in Table 5, entries 11–23) were remarkably higher for the cells employing an iodine-based electrolyte. However, thanks to its better electrochemical properties, the **E3**/**E4** redox couple allowed for higher efficiencies than those of the cells employing the other Cu(I)/Cu(II) redox mediator. Concerning the dyes, the more extended π-conjugated systems of **19a–b** provided efficiencies comparable to those of the simpler **15a**; hence, a more extended π-conjugation did not represent a real improvement in the DSSC performances. In any case, this article demonstrated the potential of abundant and cheap metals such as copper for making powerful sensitizers for DSSCs.

In 2019, Srivastava and Singh et al. [39] prepared and tested the five homoleptic dithiocarbamate Cu(II) complex dyes **20a–e**. The ligands were rather simple, and the difference was in the substituents (see Figure 10).

The UV–Vis spectra of these complexes were characterized by two absorption bands: the first around 440 nm, with a molar absorption coefficient ranging from 4.1×10^3 to 9.0×10^3 M^{-1} cm^{-1}; the second one (weaker, ε ranging from 0.70×10^2 to 1.33×10^2 M^{-1} cm^{-1}) was located around 650 nm. From the energy level diagram (vs. Ag/Ag⁺), it was possible to understand that the LUMO levels fell between −2.52 and −2.71 V and the HOMO between +0.15 and +0.33 V. Consequently, the electron injection in the conduction band of TiO₂ (−0.82 V) and the dye restoration by the I^-/I_3^- redox couple (+0.05 V) were feasible.

The measured photovoltaic performances of DSSCs fabricated with TiO₂, employing complexes **20a–e** and **N719**, and tested under AM 1.5G illumination conditions (see Table

5, entries 24–29), were higher for **20c** than for the other Cu-based compounds. This complex also had a higher J_{SC} than those of the other synthesized complexes and showed 70.7% efficiency relative to the reference **N719**. In addition, the dye loading onto the titania film was higher for **17c** than for the other dyes (2.16×10^{-7} mol cm^{-2} vs. 0.76×10^{-7}, 1.70×10^{-7}, 1.16×10^{-7}, and 0.65×10^{-7} mol cm^{-2} for **20a**, **20b**, **20c,** and **20d**) and the electron lifetimes (5.45 ms vs. 3.68, 4.58, 3.68, and 3.10 ns) were higher for **20c** than those observed for the other Cu dyes. Although these dyes were still not comparable to **N719** in terms of DSSC performances, significant results were obtained anyway, especially with **20c**. Despite the lack of one or more anchoring carboxylic groups, these dyes represented a major step in the synthesis of novel Cu sensitizers for DSSC.

In 2019, Agırtas et al. [40] synthesized a (4-tritylphenoxy) phthalocyanine ligand and coordinated it to three different metal cations (namely, Cu, Zn, and Co) to obtain complexes **21a–c** (structures in Figure 10). The goal of this study was the improvement of the DSSC performances working with strong light absorbers and in parallel the reduction of the cost of these devices.

The UV–Vis spectra of complexes **21a–c** in tetrahydrofuran (THF) showed a medium intense band around 350 nm, a weak band around 600 nm, and a strong absorption band closer to 700 nm. The calculated molar absorption coefficients for **21a**, **21b,** and **21c** were 50,973, 29,224, and 50,811 M^{-1} cm^{-1}. Each complex was soluble in THF and none of them showed aggregation phenomena.

The photovoltaic performances of complexes **21a–c** were determined under AM 1.5G irradiation, assembling the DSSCs using an FTO glass substrate, TiO$_2$, a Pt counter electrode, and with the commercial electrolyte solution Solaronix Iodolyte AN-50 (data in Table 5, entries 30–32). The Cu-based complex had the best performances; even if only 1.77% efficiency was reached in the case of complex **21a**, its broad absorption spectrum and high molar extinction coefficient represented important characteristics that the ideal dye should have. The optimization of **21a** should further improve the performances of Cu-based DSSCs.

In 2020, Agırtas et al. [41] synthesized another phthalocyanine ligand coordinated to Zn, Co, and Cu metal centers to obtain dyes **22a–c** (structures in Figure 10).

Similar to complexes **21a–c**, compounds **22a–c** were characterized by an absorption spectrum in THF constituted by three bands: a medium intense band around 350 nm, a weak one around 600 nm, and the strongest localized band close to 700 nm. Even in this case, the molar extinction coefficients were very high (26,582, 31,713, and 25,498 M^{-1} cm^{-1} for **22a–c**, respectively). In addition, in this case, the dyes did not aggregate in solution when the concentration was between 2×10^{-5} and 8×10^{-5} M.

The photovoltaic properties of the DSSCs fabricated with **22a–c** (see Table 5, entries 33–35), FTO glass, TiO$_2$, the I$^-$/I$_3^-$ redox couple, and a Pt counter electrode were tested under AM 1.5G illumination conditions. It emerged that, even in this case, the Cu complex was the best dye among the three synthesized due to its higher efficiency, J_{SC}, V_{OC}, and FF. Despite the low conversion efficiencies, the optimization of these complexes, especially the Cu-based dye **22a**, could lead to more efficient and cheaper DSSCs.

In 2020, Nyokong et al. [42] synthesized a novel asymmetric phthalocyanine ligand for chelating Cu and Zn cations (see complexes **23a–b** in Figure 10). The asymmetry of this ligand represented a major step forward with respect to the previously cited dyes **21a–c** and **22a–c**, and this was achieved by introducing two anchoring carboxylicic groups onto a phenyl ring placed on one isoindole subunit. Another peculiarity of these dyes was the presence of electron-donating *tert*-butyl groups on the other isoindole subunit, which were included to enhance the push–pull characteristics of these molecules. Another important point was the steric hindrance of this group, which was useful for reducing the tendency to aggregate. Moreover, reduced Graphene Oxide Nanosheets (rGONS) and Nitrogen-reduced Graphene Oxide Nanosheets (NrGONS) were employed in the DSSC fabrication to improve the photovoltaic performances hampering the charge recombination at the photoanode/dye/electrolyte interface.

As for complexes **21a–c** and **22a–c**, the UV–Vis spectra were constituted by a medium intense band around 350 nm, a weak one around 610 nm, and by the strongest absorption band around 670 nm. The solid-state absorption spectra of the Indium Tin Oxide (ITO)/TiO$_2$/rGONS sensitized electrode were completely different; in fact, the dye easily aggregated, provoking the broadening and flattening of the absorption bands. The energy levels were −4.04 and −3.43 eV (LUMO) and −5.87 and −5.25 eV (HOMO) for complexes **23a** and **23b**. Each dye was able to inject electrons into the TiO$_2$ conduction band, located at −4.20 eV, and to be restored by the I⁻/I$_3$⁻ redox couple (−4.89 eV).

Four DSSCs were fabricated employing ITO as conductive glass, TiO$_2$ functionalized with rGONS and NrGONS as semiconductor, complexes **23a–b,** and ITO functionalized with NrGONS as counter electrode (data in Table 5, entries 36–39). While a minor improvement was observed when the titania film was functionalized with NrGONS, an important enhancement resulted from the application of the Cu-sensitizer **23a** rather than **23b**. This work not only demonstrated the possibility of producing efficient DSSCs employing abundant metals such as Cu, but also showed that the introduction of electron-withdrawing anchoring groups and electron-donating *tert*-butyl groups in the ligand was fundamental to linking the dye to the photoanode and to observing a push–pull effect, and thereby a more efficient electron injection. Complex **23b** represented a promising candidate for applications in photovoltaic devices. In addition, the use of rGONS and NrGONS was useful for a reduced electron recombination and thus for guaranteeing better performances.

The previously cited study of Sreelatha et al. [18] published in 2020 also described the synthesis, characterization, and testing of the lawsone–Cu complex **3e** (DSSC performances in Table 1). Although its absorbance was lower than those of the Cr(III), Mn (II), Co(II), and Zn(II) complexes, the efficiencies of **3e** employing both TiO$_2$ nanoparticles and nanofibers were lower only than those of the Cr(III) and Fe(II)-based complexes, **3f** and **3g**. Even in this case, better performances were observed using the TiO$_2$ nanofibers instead of the nanoparticles. This meant that dye **3e** could also be a promising candidate for applications in DSSCs.

In 2020, Housecroft et al. published a paper [43] presenting five new bipyridinic ligands prepared by Schiff condensation between an aldehyde and a 4-R-aniline (R = H, Me, *t*Bu, OMe, and NMe$_2$). By employing the mentioned chelating ligands with the already-presented phosphonic acid anchoring ligand, the heteroleptic cuprous dyes **24a–e** were obtained though the SALSAC approach (structure in Figure 11).
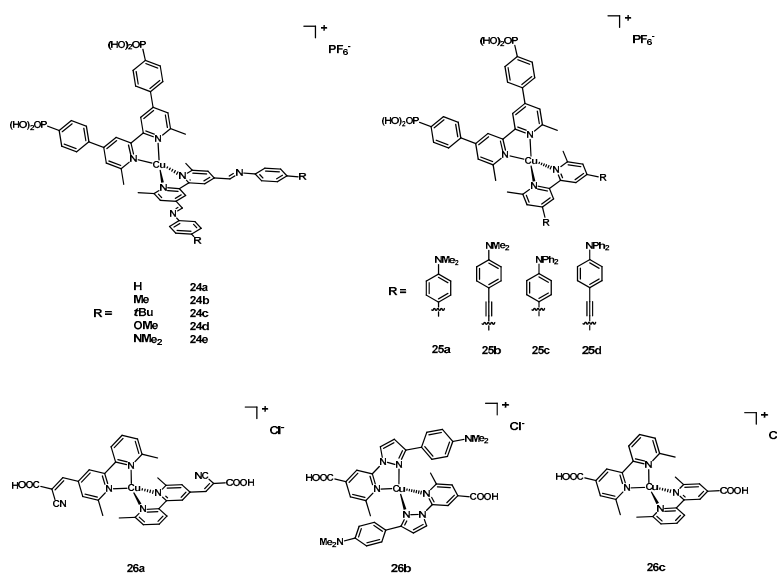

Figure 11. Structure of dyes **24a–e**, **25a–d,** and **26a–c**.

All the new compounds were tested in DSSC, achieving a FF ranging from 65% to 70%. The highest Jsc values (in both cases 4.08 mA cm^{-2}) were those of cells sensitized with **24a** and **24c**; complex **24a** also provided the best values of Voc (538 mV), efficiency (1.51%), and η_{rel} to **N719** (26%).

To clarify the effect of the introduction of the imine linker, the authors also used ligands that were different only due to the simple absence of the -C=N- group between the pyridine and the phenyl rings. In all the compared couples of the devices based on iminic and non-iminic ancillary ligands, it was pointed out that the presence of such a group was detrimental for the DSSCs' performances, leading to lower values of Jsc, Voc, and efficiency. All photovoltaic data are listed in Table 5, entries 40–55.

A different spacer, namely, an alkynyl, was published in 2020 by Constable et al. [44] in a paper in which four new chelating ligands were synthesized and tested as ligands for copper, which were to be used as dyes in DSSC. The new ligands, coupled with the anchoring phosphonic acid ligand to yield dyes **25a–d** (Figure 11), had a 4-NMe$_2$-phenyl or a 4-NPh$_2$-phenyl moiety on the pyridine ring, with or without the CC triple bond. As usual, the dyes were prepared by reacting the N^N ligands with the starting compound [Cu(CH$_3$CN)$_4$][PF$_6$], and then they were tested in different solar cells.

By comparing the photovoltaic parameters, it was clear that the introduction of the alkynyl group was not beneficial to the performances, since both the Jsc and the Voc achieved lower values (474 mA cm^{-2} and 539 mV for **25a**; 3.59 mA cm^{-2} and 514 mV for **25b**). The same trend arose from dyes **25c** and **25d**, confirming the negative effect of the alkynyl moiety on the cell parameters. Table 5, entries 56–77, reports the data for the produced solar cells.

In 2021, Inomata and Masuda et al. [45] published the three homoleptic asymmetric dyes **26a–c** (structures in Figure 11). Compounds **26a** and **26c** had two bipyridine ligands while **26b** had two 2-pyrazol-1-yl pyridines. Two anchoring carboxylic groups were present in each complex: compound **26a** had a strong electron-withdrawing cyanoacrylic acid moiety, whereas **26b–c** had two simple carboxylic groups directly linked to the pyridine rings.

The UV–Vis spectra of **26a** and **26c** in EtOH consisted of two intense absorption bands in the near UV range (**26a**: λ_{max} = 317 nm, ε = 23200 M^{-1} cm^{-1}, **26c**: λ_{max} = 312 nm, ε = 27500 M^{-1} cm^{-1}) and a less intense band in the visible range (**26a**: λ_{max} = 497 nm, ε = 9330 M^{-1} cm^{-1}, **26c**: λ_{max} = 475 nm, ε = 7480 M^{-1} cm^{-1}). The spectrum of **26b** was different, consisting of only one intense absorption band at 355 nm (ε = 25500 M^{-1} cm^{-1}) because the introduction of an electron-donating dimethylamino group significantly blue-shifted the absorption band associated with the $\pi \rightarrow \pi^*$ transition. The ΔG values of **26a** and **26c** with respect to the I$^-$/I$_3^-$ redox couple were 0.09 and 0.15 V and clearly indicated a small driving force for the dye regeneration. On the other hand, **26b** showed a much higher ΔG of 0.51 V, indicating a more efficient regeneration than those of **26a** and **26c**. DFT calculations showed that the HOMO levels were located on the Cu atom in complexes **26a** and **26c**, and on the dimethylamino group of **26b**. The LUMO levels were on the rings bearing the carboxylic group.

The photovoltaic performances of the DSSCs fabricated with **26a–c** and **N719** (see Table 6, entries 1–4) were determined under AM 1.5G irradiation conditions. Dyes **26a–b** showed poor performances, but the simpler **26c** exhibited an efficiency of 2.66%. This was because **26a** was penalized due to the small driving force and since **26b** did not have any broad absorption band in the visible region, in contrast with the other complexes. On the other hand, **26c** had its LUMO levels localized mostly on the anchoring carboxylic group, thereby increasing the conversion efficiency. Despite the quite low efficiencies observed, the simple structure of the ligands of **26c** allowed for the highest conversion efficiencies and their optimization could lead to more efficient photovoltaic devices.

Table 6. Photovoltaic data of DSSCs produced with dyes **26a–c**, **27a–d**, **28a–g**, **29a–d**, and **30a–d** [1].

Entry	Dye	Redox Couple	J_{SC} (mA cm⁻²)	V_{OC} (V)	FF	η (%)	η_{rel} (%)	Ref.
1	**26a** [2]	I⁻/I₃⁻ [3]	0.61	0.48	0.58	0.17	2.17	[45]
2	**26b** [4]	I⁻/I₃⁻ [3]	1.64	0.6	0.65	0.64	8.17	[45]
3	**26c** [2]	I⁻/I₃⁻ [3]	6.08	0.66	0.66	2.66	33.97	[45]
4	**N719** [2]	I⁻/I₃⁻ [3]	16.5	0.69	0.69	7.83		[45]
5	**27a** [5]	I⁻/I₃⁻ [6]	17.51	0.79	0.693	8.82		[46]
6	**27b** [5]	I⁻/I₃⁻ [6]	17.02	0.78	0.668	8.32		[46]
7	**27c** [5]	I⁻/I₃⁻ [6]	15.07	0.76	0.692	8.03		[46]
8	**27d** [5]	I⁻/I₃⁻ [6]	14.38	0.74	0.695	7.55		[46]
9	**28a** [7,8,9]	I⁻/I₃⁻ [10]	2.87 ± 0.10	0.550 ± 0.010	0.74 ± 0.02	1.17 ± 0.09	15.39	[47]
10	**28b** [7,8,11]	I⁻/I₃⁻ [10]	3.31 ± 0.12	0.563 ± 0.005	0.74 ± 0.02	1.38 ± 0.10	18.16	[47]
11	**28c** [7,8,11]	I⁻/I₃⁻ [10]	3.17 ± 0.11	0.555 ± 0.005	0.70 ± 0.01	1.23 ± 0.10	16.18	[47]
12	**28d** [7,8,11]	I⁻/I₃⁻ [10]	4.79 ± 0.11	0.563 ± 0.005	0.68 ± 0.02	1.81 ± 0.12	23.82	[47]
13	**28e** [7,8,11]	I⁻/I₃⁻ [10]	4.79 ± 0.07	0.565 ± 0.010	0.73 ± 0.02	2.05 ± 0.08	26.97	[47]
14	**28f** [7,8,12]	I⁻/I₃⁻ [10]	3.35 ± 0.09	0.553 ± 0.005	0.67 ± 0.02	1.24 ± 0.09	16.32	[47]
15	**25g** [7,8,11]	I⁻/I₃⁻ [10]	4.16 ± 0.10	0.566 ± 0.005	0.72 ± 0.02	1.73 ± 0.09	22.76	[47]
16	**28e** [7,11]	I⁻/I₃⁻ [13]	0.351 ± 0.050	0.512 ± 0.015	0.65 ± 0.03	0.117 ± 0.030	1.54	[47]
17	**28e** [7,11]	Co²⁺/Co³⁺ [14]	0.199 ± 0.040	0.485 ± 0.010	0.53 ± 0.08	0.052 ± 0.020	0.68	[47]
18	**28e** [7,11]	Co²⁺/Co³⁺ [15]	0.030 ± 0.006	0.343 ± 0.030	0.47 ± 0.01	0.005 ± 0.001	0.07	[47]
19	**28e** [7,11]	I⁻/I₃⁻ [12]	2.664 ± 0.030	0.560 ± 0.005	0.69 ± 0.03	1.02 ± 0.05	13.42	[47]
20	**28e** [7,11]	I⁻/I₃⁻ [10]	4.711 ± 0.050	0.605 ± 0.005	0.74 ± 0.00	2.10 ± 0.02	27.63	[47]
21	**28e** [7,11]	I⁻/I₃⁻ [10]	4.693 ± 0.100	0.622 ± 0.005	0.71 ± 0.01	2.07 ± 0.09	27.24	[47]
22	**28e** [7,11]	I⁻/I₃⁻ [16]	4.192 ± 0.110	0.577 ± 0.005	0.72 ± 0.01	1.74 ± 0.10	22.89	[47]
23	**N719** [7,8]	I⁻/I₃⁻ [10]	17.81 ± 0.09	0.700 ± 0.005	0.61 ± 0.01	7.60 ± 0.21		[47]
24	**29a** [17]	I⁻/I₃⁻ [18]	9.80	0.69	0.705	4.77		[48]
25	**29b** [17]	I⁻/I₃⁻ [18]	10.28	0.73	0.709	5.30		[48]
26	**29c** [17]	I⁻/I₃⁻ [18]	14.86	0.79	0.720	8.45		[48]
27	**29d** [17]	I⁻/I₃⁻ [18]	14.94	0.79	0.726	8.59		[48]
28	**30a** [17]	I⁻/I₃⁻ [19]	17.45	0.78	0.704	9.03		[49]
29	**30b** [17]	I⁻/I₃⁻ [19]	14.75	0.76	0.704	8.02		[49]
30	**30c** [17]	I⁻/I₃⁻ [19]	13.94	0.74	0.717	6.82		[49]
31	**30d** [17]	I⁻/I₃⁻ [19]	12.00	0.75	0.669	6.12		[49]

[1] using FTO as conductive oxide, TiO₂ as semiconductor, Pt as counter-electrode, and under AM 1.5G-simulated light source (100 mW cm⁻²) if not differently specified. [2] 0.3 mM dye in EtOH. [3] 0.1 M LiI + 0.05 M I₂ + 0.6 M DMPII + 0.5 M TBP in ACN. [4] 0.3 mM dye in MeOH. [5] 0.05 mM in DMF. [6] 0.5 M LiI + 0.05 M I₂ + 0.5 M TBP. [7] use of Pilkington TEC15 as conductive glass. [8] tested two days after the fabrication.[9] 1 mM anchoring ligand in MeOH; then 1 mM [Cu(CH₃CN)₄][PF₆] + 2 mM anchoring ligand in MeOH. [10] 0.025 M LiI + 0.04 M I₂ + 0.65 M BMII + 0.28 M TBP in ACN:BuCN 85:15 *v/v*. [11] 1 mM anchoring ligand in MeOH, then 1 mM [Cu(CH₃CN)₄][PF₆] + 1 mM Cu homoleptic complex in ACN. [12] 1 mM anchoring ligand in MeOH, then 1 mM [Cu(CH₃CN)₄][PF₆] + 2 mM ancillary ligand in ACN. [13] 0.1 M LiI + 0.05 M I₂ + 0.6 M BMII + 0.5 M methylbenzimidazole in 3-methoxypropionitrile. [14] 0.22 M [Co(bpy)₃]²⁺ + 0.05 M [Co(bpy)₃]³⁺ + 0.2 M TBP + 0.1 M LiClO₄ in ACN. [15] 0.22 M [Co(bpy)₃]²⁺ + 0.05 M [Co(bpy)₃]³⁺ + 0.1 M LiClO₄ in ACN. [16] 0.1 M LiI + 0.05 M I₂ + 1.0 M BMII + 0.5 M TBP in ACN:BuCN 85:15 *v/v*. [17] 0.2 mM dye in DMF. [18] 0.05 M LiI + 0.6 M I₂ + 0.1 M DMPII + 0.5 M TBP in ACN. [19] 0.1 M LiI + 0.05 M I₂ + 0.6 M DMPII + 0.5 M TBP in ACN.

In 2021, Zhong et al. [46] synthesized four novel dyes (**27a–d**, structures in Figure 12), employing Cd(II), Zn(II), Cu(II), and Co(II) as metal centers. In addition, in this case, an additional electron acceptor was placed between the donor and the conjugated π-bridge to reduce the intramolecular charge recombination between the donor and acceptor. In particular, a single donor was connected to two metal centers in order to obtain a D-(A-π-A)₂ system. The chosen donor was a bis(5-(2-ethyloctyl)thiophen-2-yl)benzo [1,2-b:4,5-b0]dithiophene (thienylbenzo-[1,2-b:4,5-b']-dithiophene, BDTT) moiety and the acceptors were based on 8-hydroxyquinoline ligands. The anchoring group was a cyanoacrylic acid.
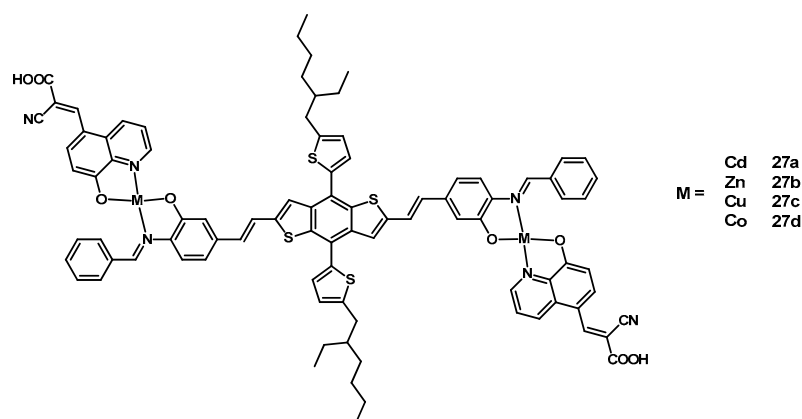
Figure 12. Structure of dyes **27a–d**.

The UV–Vis spectra of the novel dyes consisted of two intense and broad absorption bands: the first ranging from 481 to 508 nm, and the second from 366 to 432 nm. The maximum molar extinction coefficients had values of 19,520, 18,418, 17,565, and 16,880 M^{-1} cm^{-1} for compounds **27a–d**, and they were associated with the absorption bands between 481 and 508 nm. The Cd(II) complex **27a** had a more intense absorption band than the Cu(II) one (**27c**) because of its larger radius, which strengthened the interaction with the ligand. In addition, the spectra of the metal complexes without the BDTT parts were recorded; however, they showed only a single absorption band between 350 and 400 nm because of the absence of a strong light absorber such as the BDTT group that was responsible for the broader and strongly red-shifted band around 500 nm described before. From the electrochemical characterization it emerged that the LUMO levels were from −3.309 to −3.322 eV, while the HOMO levels were between −5.347 and −5.465 eV, indicating a feasible electron injection in the conduction band of TiO_2 (−4.26 eV) and an efficient dye regeneration by the I^-/I_3^- redox couple (−4.83 eV). Due to the exposure to sunlight, a TGA under a N_2 atmosphere was carried out to understand at which temperature the dye degradation takes place. It emerged that the onset temperatures were 340, 323, 328, and 309 °C for dyes **27a–d**; therefore, these dyes were stable enough for applications in DSSCs.

Four DSSCs were assembled using these dyes and were tested under AM 1.5G illumination conditions (data in Table 6, entries 5–8). The Cu-based dye **27c** showed a lower efficiency, V_{OC}, and J_{SC} than **27a–b** (based on Cd an Zn), but a higher FF, indicating that the influence of different metal cations was very important for achieving a high efficiency. In any case, interesting conversion performances were observed for the Cu-based dye **27c**, and its optimization may lead to improved devices.

In 2022, Gardner et al. [47] synthesized seven novel Cu dyes, namely, **28a–g** (see Figure 13), bearing simple bipyridine and phenanthroline ligands. Compound **28a** was a homoleptic Cu(I) complex with two bipyridine ligands, each containing two anchoring carboxylic groups. The other ones were characterized by an anchoring bipyridine and an ancillary phenanthroline with different substituents. Only **28f** had a bipyridine ancillary ligand.
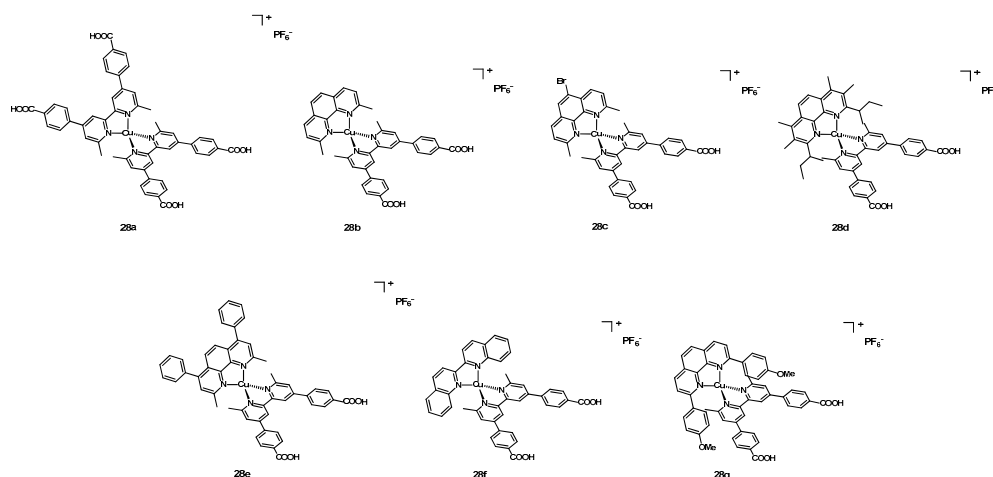
Figure 13. Structure of dyes **28a–g**.

The UV–Vis spectra of the TiO$_2$ of complexes **28a–e** and **28g** showed an absorption band between 450 and 500 nm, which was significantly red-shifted to about 520–550 nm in the case of **28f**. The HOMO levels were between +0.83 and +0.96 eV vs. a Normal Hydrogen Electrode (NHE), whereas the LUMO levels were between −1.00 and −1.45 eV vs. an NHE. Since the TiO$_2$ conduction band and the redox potential of the I$^-$/I$_3^-$ redox couple were placed at about −0.5 and +0.5 eV vs. an NHE, both the electron injection and dye regeneration were possible.

Complexes **28a–g** were deposited over the titania layer by immersing the electrode into a MeOH solution of the anchoring ligand. After that, the electrode was washed and immersed in another solution containing the homoleptic complex with the desired ligand in ACN or in a solution of the desired ligand plus [Cu(CH$_3$CN)$_4$][PF$_6$] in ACN (the SAL-SAC approach; more detailed information can be found in Table 6, entries 9–23, together with the photovoltaic performances of these cells). Both I$^-$/I$_3^-$ and Co(II)/Co(III) couples were tested, but the second one bleached the cell, consequently leading to lower performances. Among the cuprous sensitizers, **28e** showed not only the best efficiency, but also the best J$_{SC}$. Even if these dyes had lower performances than the reference **N719**, they represented promising candidates for applications in photovoltaic devices when employed with the I$^-$/I$_3^-$ electrolytes.

In 2022, Zhong et al. [48] synthesized two new polymeric ligands for chelating Cu(II) and Cd(II) cations, obtaining the polymeric dyes **29a–d** (structures in Figure 14). In addition, in this case, D-A-π-A dyes were synthesized to achieve better performances than those of the commonly used D-π-A systems. The chosen donors were 1,4-dioctyloxybenzene and BDTT, while the ligands were derivatives of 8-hydroxyquinoline (bearing an anchoring cyanoacrylic acid) and iminic derivatives of salicylaldehyde.
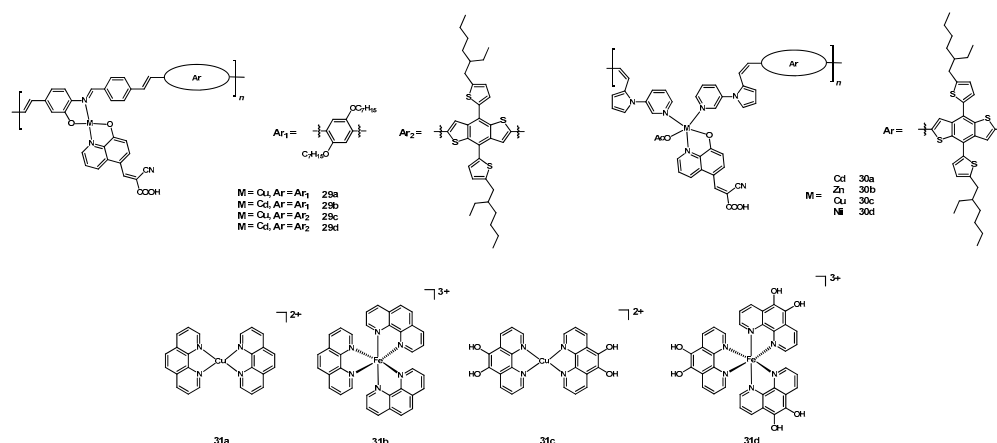
Figure 14. Structure of dyes **29a–d**, **30a–d,** and **31a–d**.

The UV–Vis spectra of the polymeric complexes **29a–d** were characterized by two absorption bands: the first one between 300 and 400 nm; the second one around 450 nm in the case of **29a–b,** and between 510 and 530 nm for **29c–d**. The second band was stronger than the first one and was associated with a high molar absorption coefficient (18,254, 18,741, 19,858 and 20,188 M^{-1} cm^{-1} for **29a–d**). The dyes employing the thienylbenzo-[1,2-b:4,5-b']-dithiophene moiety as electron donor had a higher molar extinction coefficient than those based on 1,4-dioctyloxybenzene. The HOMO levels were between −5.224 and −5.333 eV while the LUMO levels were between −3.125 and −3.229 eV, so each dye was capable of injecting electrons into the TiO_2 conduction band (−4.26 eV) and could be regenerated by the I^-/I_3^- redox couple (−4.83 eV). The thermal stability of dyes **29a–d** was tested through TGA: the onset temperatures were higher than 300 °C, except for **29a**, whose thermal degradation started at 246 °C. In any case, the high onset temperatures indicated that compounds **29a–d** were stable enough to be used in DSSCs.

The photovoltaic performances of the DSSCs fabricated with **29a–d** are summarized in Table 6, entries 24–27. As in the case of the absorption spectra, higher J_{SC}, V_{OC}, FF, and, consequently, efficiencies were observed when the thienylbenzo-[1,2-b:4,5-b']-dithiophene moiety was present. The Cd complexes showed higher efficiencies than the Cu ones due to the lower E_g (2.208 vs. 2.124 for **29a–b** and 2.035 vs. 2.002 for **29c** and **29d**). Nevertheless, the difference was minimal and so the Cu complexes **29a** and **29c** were promising candidates for applications in DSSCs.

In 2022, Zhong et al. [49] also synthesized a novel polymeric ligand for Cd, Zn, Cu, and Ni metal centers (see complexes **30a–d** in Figure 14). In addition, in this case, a D-A-π-A system was produced to reduce the intramolecular charge recombination between the donor and acceptor. BDTT was used as electron donor, while the ligands were an 8-hydroxyquinoline derivative and two pyridines.

Considering the UV–Vis spectra of complexes **30a–d**, the maximum absorption wavelengths were at 506, 488, 478, and 464 nm, and were characterized by molar absorption coefficients between 18,000 and 23,500 M^{-1} cm^{-1}, following the order **30d** < **30c** < **30b** < **30a**. The HOMO and LUMO levels were between −3.269 and −3.314 eV, and between −5.336 and −5.475 eV, respectively. Each dye could inject electrons into the conduction band of the titania layer (−4.26 eV) and could be regenerated by the I^-/I_3^- redox couple (−4.83 eV). The TGA of the polymeric complexes **30a–d** under a nitrogen atmosphere showed a high stability, with the onset temperatures of 314, 296, 287, and 268 °C, respectively.

From the photovoltaic characterization of complexes **30a–d** (data in Table 6, entries 28–31) it emerged that the J_{SC} decreased when moving from **30a** to **30d**. V_{OC} and FF were more constant; the efficiency followed the same trend of the J_{SC}, and the higher perfor-

mances of **30a** and **30b** were associated with the larger radius of the metal cation. Although the Cu complex had lower performances than the Cd and Zn complexes, its optimization could lead to improved DSSC devices.

4. Employing Cu and Fe Dyes Together

In 2019, Çakar [50] synthesized four Cu and Fe complexes bearing simple phenanthrolinic ligands. Dyes **31a–b** had two unsubstituted phenanthrolines, while **31c–d** presented two 1,10-phenanthroline-5,6-diol ligands (see Figure 14). Iron and copper dyes were employed both alone and in combination as sensitizers for DSSCs.

The UV–Vis spectra were characterized by two absorption bands around 250 and 450 nm. The band around 450 nm was much less intense in the spectra of the mixtures of **31a–b** and **31c–d** in different ratios. The HOMO and LUMO of each dye ranged from −5.25 to −5.44 eV, and from −3.26 to 3.82 eV, respectively. Therefore, the electron injection in the TiO_2 conduction band and the dye regeneration by the I^-/I_3^- redox couple was able to take place efficiently.

The photovoltaic performances of 19 DSSCs fabricated with dyes **31a–d** and the reference dye **N719** are summarized in Table 7. Considering the cells fabricated using a single dye, the Cu-based dyes **31a** and **31c** showed better performances than the Fe-based **31b** and **31d**. Even the effects of different pH values on the performances were tested, and it emerged that each Cu dye had a higher efficiency at pH 7, whereas the Fe complexes were more efficient at pH 3.5. Some DSSCs fabricated with the dyes **31a–b** and **31c–d** together in different ratios (Cu:Fe 1:1, 2:1 and 1:2) were also fabricated. Differently from the previously mentioned devices, working with a mixture of two different sensitizers promoted an improvement in the V_{OC}, and especially in the J_{SC} and the photovoltaic efficiency. The best results were obtained working with the 2:1 Cu:Fe ratio. For each sensitizer or mixture, a minor improvement was observed switching to the 1,10-phenanthroline-5,6-diol ligands because of the stronger interaction with the titania layer. Although a comparable efficiency to that of the reference dye **N719** was still not reached, the combination of Cu and Fe dyes represented a major step forward with respect to the different metal complexes employed alone. The complexes described here are very simple, and their optimization could lead to much more efficient photovoltaic devices.

Table 7. Photovoltaic data of DSSCs produced with dyes **31a–d** [1].

Entry	Dye	Redox Couple	J_{SC} (mA cm^{-2})	V_{OC} (V)	FF	η (%)	η_{rel} (%)	Ref.
1	**31a**: **31b**: 1:1	I^-/I_3^- [2]	8.78	0.74	0.50	3.25	40.88	[50]
2	**31a**: **31b**: 2:1	I^-/I_3^- [2]	8.96	0.76	0.51	3.47	43.65	[50]
3	**31a**: **31b**: 1:2	I^-/I_3^- [2]	8.30	0.74	0.50	3.07	38.62	[50]
4	**31c**: **31d** 1:1	I^-/I_3^- [2]	9.02	0.75	0.51	3.45	43.40	[50]
5	**31c**: **31d** 2:1	I^-/I_3^- [2]	9.31	0.78	0.51	3.70	46.54	[50]
6	**31c**: **31d** 1:2	I^-/I_3^- [2]	8.14	0.75	0.51	3.11	39.12	[50]
7	**31a**	I^-/I_3^- [2]	5.10	0.55	0.54	1.49	18.74	[50]
8	**31a**	I^-/I_3^- [2]	7.06	0.74	0.50	2.61	32.83	[50]
9	**31a**	I^-/I_3^- [2]	6.95	0.73	0.49	2.48	31.19	[50]
10	**31b**	I^-/I_3^- [2]	5.14	0.74	0.49	1.86	23.40	[50]
11	**31b**	I^-/I_3^- [2]	4.68	0.72	0.50	1.63	20.50	[50]
12	**31b**	I^-/I_3^- [2]	4.65	0.70	0.48	1.56	19.62	[50]
13	**31c**	I^-/I_3^- [2]	5.31	0.61	0.50	1.61	20.25	[50]
14	**31c**	I^-/I_3^- [2]	7.32	0.75	0.51	2.80	35.22	[50]
15	**31c**	I^-/I_3^- [2]	7.17	0.73	0.49	2.56	32.20	[50]
16	**31d**	I^-/I_3^- [2]	5.39	0.76	0.50	2.05	25.79	[50]
17	**31d**	I^-/I_3^- [2]	4.86	0.71	0.49	1.75	22.01	[50]
18	**31d**	I^-/I_3^- [2]	5.06	0.73	0.50	1.85	23.27	[50]
19	**N719**	I^-/I_3^- [2]	13.85	0.95	0.60	7.95		[50]

[1] using FTO as conductive oxide, TiO_2 as semiconductor, Pt as counter-electrode, and under AM 1.5G-simulated light source (100 mW cm^{-2}) if not differently specified. [2] 0.1 M LiI + 0.05 M I_2 + 0.5 M TBP in ACN.

5. Conclusions

This review allowed us to show the most recent advances in the development of novel sensitizers for dye-sensitized solar cells based on cheaper and earth-abundant iron and copper as potential replacements for the rarer and more expensive ruthenium.

The discussed articles describe a wide variety of ancillary and anchoring ligands, including phenanthrolines, bipyridines, 8-hydroxyquinolines, 2,6-bis(3-methyl-1*H*-3λ^4-imidazol-1-yl)pyridines, commercially available organic dyes (like methyl orange), etc. Moreover, many different approaches were employed to synthesize increasingly better performing dyes, hence the use of increasingly efficient cells, such as the use of anchoring phosphonyl groups, the synthesis of polymeric dyes, and the SALSAC method for the synthesis of the ligands onto a previously functionalized titania film. Iron and copper were also used together, and in combination with other abundant and cheap metals such as Cd, Zn and Hg, in an attempt to push the photovoltaic efficiencies towards even higher values.

As mentioned several times before, both Cu- and Fe-based complexes are currently still not comparable with the ruthenium reference dye **N719**. However, interesting results were obtained with both the discussed alternative solutions. Among the iron-based dyes, the ferrocenyl-chalcone dye with azine spacers and bearing a hydroxyl group (compound **10a**) was particularly interesting. In fact, it led to an efficiency of 5.88%, which was close to that of **N719** (6.32%), guaranteeing a relative efficiency of 93.04%. It was also shown that the rather low efficiencies—hardly above 2%—obtained employing the iron complexes could be dramatically improved by synthesizing molecules containing an iron and another metal center at the same time, or by employing an iron complex together with another metal complex in the same DSSC. Two striking examples were the 1,1'-bis(diphenylphosphino)ferrocene Ni(II) dithiolate **12d** with 5.05% efficiency (79.91% relative efficiency to **N719**) and the Zn-ferrocene complex **13a** with 2.79% efficiency (66.43% relative efficiency to **N719**). The DSSCs fabricated with the latter were also improved by coupling it with **N719**, reaching an efficiency of 5.71% (a 135.95% increase in relative efficiency compared to **N719** alone). Regarding the copper dyes, of particular interest were the polymeric sensitizers with a D-A-π-A structure, which greatly enhanced the photovoltaic performances with respect to the classical D-π-A structures, especially when the thienylbenzo-[1,2-b:4,5-b']-dithiophene was employed as a donor, leading to photovoltaic efficiencies up to 8.45%. Despite their much lower performances, the full-copper DSSCs should also be mentioned because they demonstrated the possibility of eliminating the dependence on the classical I^-/I_3^- redox couple using simple and cheap copper complexes with phenanthrolinic ligands.

The studies included in this review demonstrated the feasibility of dye-sensitized solar cells employing copper and iron dyes alone or in combination with other cheap and abundant metals, which could achieve remarkable efficiencies. In conclusion, the proper optimization of the sensitizers, together with those of the electrolyte and of the titania layer, will likely lead to the development of highly performing and cheap photovoltaic devices for future applications on a much larger scale.

Author Contributions: Writing—original draft preparation, F.F.; writing—review and editing, A.C., C.D., F.F., L.M. All authors have read and agreed to the published version of the manuscript.

Institutional Review Board Statement: Not applicable

Informed Consent Statement: not applicable.

Data Availability Statement: Not applicable.

Conflicts of Interest: The authors declare no conflict of interest.

References

1. Cho, A. Energy's Tricky Tradeoffs. *Science* **2010**, *329*, 786–787. https://doi.org/10.1126/SCIENCE.329.5993.786/ASSET/CC593E56-8678-4DA2-A3DA-A8F63A57F494/ASSETS/SCIENCE.329.5993.786.FP.PNG.
2. O'Regan, B.; Grätzel, M. A Low-Cost, High-Efficiency Solar Cell Based on Dye-Sensitized Colloidal TiO$_2$ Films. *Nature* **1991**, *353*, 737–740. https://doi.org/10.1038/353737a0.
3. Mazloum-Ardakani, M.; Arazi, R. Improving the Effective Photovoltaic Performance in Dye-Sensitized Solar Cells Using an Azobenzenecarboxylic Acid-Based System. *Heliyon* **2019**, *5*, e01444. https://doi.org/10.1016/J.HELIYON.2019.E01444.
4. Colombo, A.; Dragonetti, C.; Magni, M.; Meroni, D.; Ugo, R.; Marotta, G.; Grazia Lobello, M.; Salvatori, P.; de Angelis, F. New Thiocyanate-Free Ruthenium(II) Sensitizers with Different Pyrid-2-Yl Tetrazolate Ligands for Dye-Sensitized Solar Cells. *Dalton Trans.* **2015**, *44*, 11788–11796. https://doi.org/10.1039/C5DT01216C.
5. Colombo, A.; Dragonetti, C.; Valore, A.; Coluccini, C.; Manfredi, N.; Abbotto, A. Thiocyanate-Free Ruthenium(II) 2,2'-Bipyridyl Complexes for Dye-Sensitized Solar Cells. *Polyhedron* **2014**, *82*, 50–56. https://doi.org/10.1016/J.POLY.2014.04.048.
6. Dragonetti, C.; Valore, A.; Colombo, A.; Magni, M.; Mussini, P.; Roberto, D.; Ugo, R.; Valsecchi, A.; Trifiletti, V.; Manfredi, N.; et al. Ruthenium Oxyquinolate Complexes for Dye-Sensitized Solar Cells. *Inorg. Chim. Acta* **2013**, *405*, 98–104. https://doi.org/10.1016/J.ICA.2013.05.006.
7. Dragonetti, C.; Colombo, A.; Magni, M.; Mussini, P.; Nisic, F.; Roberto, D.; Ugo, R.; Valore, A.; Valsecchi, A.; Salvatori, P.; et al. Thiocyanate-Free Ruthenium(II) Sensitizer with a Pyrid-2-Yltetrazolate Ligand for Dye-Sensitized Solar Cells. *Inorg. Chem.* **2013**, *52*, 10723–10725. https://doi.org/10.1021/IC401794G/SUPPL_FILE/IC401794G_SI_001.PDF.
8. Abbotto, A.; Coluccini, C.; Dell'Orto, E.; Manfredi, N.; Trifiletti, V.; Salamone, M.M.; Ruffo, R.; Acciarri, M.; Colombo, A.; Dragonetti, C.; et al. Thiocyanate-Free Cyclometalated Ruthenium Sensitizers for Solar Cells Based on Heteroaromatic-Substituted 2-Arylpyridines. *Dalton Trans.* **2012**, *41*, 11731–11738. https://doi.org/10.1039/C2DT31551C.
9. Pogozhev, D.V.; Bezdek, M.J.; Schauer, P.A.; Berlinguette, C.P. Ruthenium(II) Complexes Bearing a Naphthalimide Fragment: A Modular Dye Platform for the Dye-Sensitized Solar Cell. *Inorg. Chem.* **2013**, *52*, 3001–3006. https://doi.org/10.1021/IC3024524/SUPPL_FILE/IC3024524_SI_001.PDF.
10. Bomben, P.G.; Borau-Garcia, J.; Berlinguette, C.P. Three Is Not a Crowd: Efficient Sensitization of TiO$_2$ by a Bulky Trichromic Trisheteroleptic Cycloruthenated Dye. *Chem. Commun.* **2012**, *48*, 5599–5601. https://doi.org/10.1039/C2CC00136E.
11. Arnold, J.; Mindiola, D.; Agapie, T.; Love, J.; Dincă, M.; Dauth, A.; Love, J.A.; Stacey, T.E.; Fredrickson, D.C.; Robson, K.C.D.; et al. Cycloruthenated Sensitizers: Improving the Dye-Sensitized Solar Cell with Classical Inorganic Chemistry Principles. *Dalton Trans.* **2012**, *41*, 7814–7829. https://doi.org/10.1039/C2DT30825H.
12. Bomben, P.G.; Koivisto, B.D.; Berlinguette, C.P. Cyclometalated Ru Complexes of Type [RuII(N^N) 2(C^N)]z: Physicochemical Response to Substituents Installed on the Anionic Ligand. *Inorg. Chem.* **2010**, *49*, 4960–4971. https://doi.org/10.1021/IC100063C/SUPPL_FILE/IC100063C_SI_001.PDF.
13. Bomben, P.G.; Robson, K.C.D.; Sedach, P.A.; Berlinguette, C.P. On the Viability of Cyclometalated Ru(II) Complexes for Light-Harvesting Applications. *Inorg. Chem.* **2009**, *48*, 9631–9643. https://doi.org/10.1021/IC900653Q/SUPPL_FILE/IC900653Q_SI_001.PDF.
14. See, C.E.; Housecroft, E.; Housecroft, C.E.; Constable, E.C. Solar Energy Conversion Using First Row D-Block Metal Coordination Compound Sensitizers and Redox Mediators. *Chem. Sci.* **2022**, *13*, 1225–1262. https://doi.org/10.1039/D1SC06828H.
15. Ferrere, S. New Photosensitizers Based upon [FeII(L)2(CN)2] and [FeIIL3], Where L Is Substituted 2,2'-Bipyridine. *Inorg. Chim. Acta* **2002**, *329*, 79–92. https://doi.org/10.1016/S0020-1693(01)00743-5.
16. Ghosh, A.; Mishra, S.; Giri, S.; Mobin, S.M.; Bera, A.; Chatterjee, S. Electrolyte-Free Dye-Sensitized Solar Cell with High Open Circuit Voltage Using a Bifunctional Ferrocene-Based Cyanovinyl Molecule as Dye and Redox Couple. *Organometallics* **2018**, *37*, 1999–2002. https://doi.org/10.1021/acs.organomet.8b00104.
17. Anizaim, A.H.; Zainuri, D.A.; Zaini, M.F.; Razak, I.A.; Bakhtiar, H.; Arshad, S. Comparative Analyses of New Donor-π-Acceptor Ferrocenyl-Chalcones Containing Fluoro and Methoxy-Fluoro Acceptor Units as Synthesized Dyes for Organic Solar Cell Material. *PLoS ONE* **2020**, *15*, e0241113. https://doi.org/10.1371/journal.pone.0241113.
18. Jinchu, I.; Sreekala, C.O.; Sreelatha, K.S. Lawsone Metal Complex as an Effective Sensitizer for Dye Sensitized Solar Cells. In *Proceedings of the Materials Today: Proceedings*; Elsevier Ltd.: Amsterdam, The Netherlands, 2019; Volume 33, pp. 1356–1360.
19. Setyawati, H.; Hadi, M.S.; Darmokoesoemo, H.; Murwani, I.K.; Permana, A.J.; Rochman, F. Modification of Methyl Orange Dye as a Light Harvester on Solar Cell. In Proceedings of the IOP Conference Series: Earth and Environmental Science; Institute of Physics Publishing, 2020; Volume 456.
20. Anizaim, A.H.; Zaini, M.F.; Razak, I.A.; Arshad, S. Insight into the Impact of the Substituent Modification on the Photovoltaic Performance of Ferrocenyl Chalcones Based DSSCs. *J. Solid State Chem.* **2021**, *304*, 122551. https://doi.org/10.1016/j.jssc.2021.122551.
21. Lindh, L.; Gordivska, O.; Persson, S.; Michaels, H.; Fan, H.; Chábera, P.; Rosemann, N.W.; Gupta, A.K.; Benesperi, I.; Uhlig, J.; et al. Dye-Sensitized Solar Cells Based on Fe N-Heterocyclic Carbene Photosensitizers with Improved Rod-like Push-Pull Functionality. *Chem. Sci.* **2021**, *12*, 16035–16053. https://doi.org/10.1039/d1sc02963k.

22. Marri, A.R.; Marchini, E.; Cabanes, V.D.; Argazzi, R.; Pastore, M.; Caramori, S.; Bignozzi, C.A.; Gros, P.C. A Series of Iron(II)-NHC Sensitizers with Remarkable Power Conversion Efficiency in Photoelectrochemical Cells**. *Chem. Eur. J.* **2021**, *27*, 16260–16269. https://doi.org/10.1002/chem.202103178.

23. Reddy Marri, A.; Marchini, E.; Cabanes, V.D.; Argazzi, R.; Pastore, M.; Caramori, S.; Gros, P.C. Record Power Conversion Efficiencies for Iron(Ii)-NHC-Sensitized DSSCs from Rational Molecular Engineering and Electrolyte Optimization. *J. Mater. Chem. A* **2021**, *9*, 3540–3554. https://doi.org/10.1039/d0ta10841c.

24. Setyawati, H.; Darmokoesoemo, H.; Murwani, I.K. Dye-Sensitized Solar Cells with Napthol Blue Black as Dye Sensitizer. In *Proceedings of the Journal of Physics: Conference Series*; IOP Publishing Ltd.: Bristol, UK, 2021; Volume 1918.

25. Singh, A.; Kociok-Köhn, G.; Chauhan, R.; Muddassir, M.; Gosavi, S.W.; Kumar, A. Ferrocene Appended Asymmetric Sensitizers with Azine Spacers with Phenolic/Nitro Anchors for Dye-Sensitized Solar Cells. *J. Mol. Struct.* **2022**, *1249*, 131630. https://doi.org/10.1016/j.molstruc.2021.131630.

26. Ting, J.; Yusong, B.; Peng, Z.; Therien, M.J. Electronic Structure and Photophysics of a Supermolecular Iron Complex Having a Long MLCT-State Lifetime and Panchromatic Absorption. *Proc. Natl. Acad. Sci. USA* **2020**, *117*, 20430–20437. https://doi.org/10.1073/pnas.2009996117/-/DCSupplemental.

27. Singh, A.; Dutta, A.; Srivastava, D.; Kociok-Köhn, G.; Chauhan, R.; Gosavi, S.W.; Kumar, A.; Muddassir, M. Effect of Different Aromatic Groups on Photovoltaic Performance of 1,1'-Bis (Diphenylphosphino)Ferrocene Functionalized Ni (II) Dithiolates as Sensitizers in Dye Sensitized Solar Cells. *Appl. Organomet. Chem.* **2021**, *35*, e6402. https://doi.org/10.1002/aoc.6402.

28. Gautam, C.; Singh, A.; Gosavi, S.W.; Chauhan, R.; Sharma, V.K.; Alarifi, A.; Afzal, M.; Muddassir, M.; Kumar, A. Ferrocenyl-2-Pyridylimine Derived D10-Configuration Complexes as Prospective Co-Sensitizers in Dye Sensitized Solar Cells. *Appl. Organomet. Chem.* **2022**, *36*, e6608. https://doi.org/10.1002/aoc.6608.

29. Xiao, L.; Liu, Y.; Xiu, Q.; Zhang, L.; Guo, L.; Zhang, H.; Zhong, C. Novel Polymeric Metal Complexes as Dye Sensitizers for Dye-Sensitized Solar Cells Based on Poly Thiophene Containing Complexes of 8-Hydroxyquinoline with Zn(II),Cu(II) and Eu(III) in the Side Chain. *Tetrahedron* **2010**, *66*, 2835–2842. https://doi.org/10.1016/J.TET.2010.02.039.

30. Colombo, A.; Dragonetti, C.; Roberto, D.; Fagnani, F. Copper Complexes as Alternative Redox Mediators in Dye-Sensitized Solar Cells. *Molecules* **2021**, *26*, 194. https://doi.org/10.3390/MOLECULES26010194.

31. Dragonetti, C.; Magni, M.; Colombo, A.; Melchiorre, F.; Biagini, P.; Roberto, D. Coupling of a Copper Dye with a Copper Electrolyte: A Fascinating Springboard for Sustainable Dye-Sensitized Solar Cells. *ACS Appl. Energy Mater.* **2018**, *1*, 751–756. https://doi.org/10.1021/acsaem.7b00196.

32. Büttner, A.; Brauchli, S.Y.; Constable, E.C.; Housecroft, C.E. Effects of Introducing Methoxy Groups into the Ancillary Ligands in Bis(Diimine) Copper(i) Dyes for Dye-Sensitized Solar Cells. *Inorganics* **2018**, *6*, 40. https://doi.org/10.3390/inorganics6020040.

33. Karpacheva, M.; Malzner, F.J.; Wobill, C.; Büttner, A.; Constable, E.C.; Housecroft, C.E. Cuprophilia: Dye-Sensitized Solar Cells with Copper(I) Dyes and Copper(I)/(II) Redox Shuttles. *Dyes Pigment.* **2018**, *156*, 410–416. https://doi.org/10.1016/j.dyepig.2018.04.033.

34. Malzner, F.J.; Housecroft, C.E.; Constable, E.C. The Versatile SALSAC Approach to Heteroleptic Copper(I) Dye Assembly in Dye-Sensitized Solar Cells. *Inorganics* **2018**, *6*, 57. https://doi.org/10.3390/inorganics6020057.

35. Stephens, A.J.; Malzner, F.J.; Constable, E.C.; Housecroft, C.E. The Influence of Phosphonic Acid Protonation State on the Efficiency of Bis(Diimine)Copper(i) Dye-Sensitized Solar Cells. *Sustain. Energy Fuels* **2018**, *2*, 786–794. https://doi.org/10.1039/c7se00586e.

36. Xia, C.; Liu, Y.; Wan, T.; Xu, Z.; Wen, G.; Tang, S.; Wang, K.; Zhong, C. D-A-π-A Dye-Sensitizers with Cd (II) or Cu (II) Complex as Auxiliary Electron Acceptor. *Opt. Mater.* **2018**, *77*, 140–147. https://doi.org/10.1016/j.optmat.2018.01.022.

37. Colombo, A.; Dragonetti, C.; Fagnani, F.; Roberto, D.; Melchiorre, F.; Biagini, P. Improving the Efficiency of Copper-Dye-Sensitized Solar Cells by Manipulating the Electrolyte Solution. *Dalton Trans.* **2019**, *48*, 9818–9823. https://doi.org/10.1039/c9dt01448a.

38. Dragonetti, C.; Magni, M.; Colombo, A.; Fagnani, F.; Roberto, D.; Melchiorre, F.; Biagini, P.; Fantacci, S. Towards Efficient Sustainable Full-Copper Dye-Sensitized Solar Cells. *Dalton Trans.* **2019**, *48*, 9703–9711. https://doi.org/10.1039/c9dt00790c.

39. Manar, K.K.; Kumari, K.; Yadav, C.L.; Srivastava, P.; Drew, M.G.; Singh, N. Preparation, Characterization and Photosensitizing Activities of Homoleptic Cu(II) Dithiocarbamates in TiO2-Based DSSC. *ChemistrySelect* **2019**, *4*, 11140–11148. https://doi.org/10.1002/slct.201902517.

40. Güngördü Solğun, D.; Horoz, S.; Ağırtaş, M.S. Synthesis of Novel Tetra (4-Tritylphenoxy) Substituted Metallophthalocyanines and Investigation of Their Aggregation, Photovoltaic, Solar Cell Properties. *Inorg. Nano-Met. Chem.* **2018**, *48*, 508–514. https://doi.org/10.1080/24701556.2019.1572624.

41. Ağirtaş, M.S.; Güngördü Solğun, D.; Yildiko, Ü.; Özkartal, A. Design of Novel Substituted Phthalocyanines; Synthesis and Fluorescence, DFT, Photovoltaic Properties. *Turk. J. Chem.* **2020**, *44*, 1574–1586. https://doi.org/10.3906/kim-2007-40.

42. Chindeka, F.; Mashazi, P.; Britton, J.; Oluwole, D.O.; Mapukata, S.; Nyokong, T. Fabrication of Dye-Sensitized Solar Cells Based on Push-Pull Asymmetrical Substituted Zinc and Copper Phthalocyanines and Reduced Graphene Oxide Nanosheets. *J. Photochem. Photobiol. A* **2020**, *399*, 112612. https://doi.org/10.1016/j.jphotochem.2020.112612.

43. Lüthi, E.; Cortés, P.A.F.; Prescimone, A.; Constable, E.C.; Housecroft, C.E. Schiff Base Ancillary Ligands in Bis(Diimine) Copper(i) Dye-sensitized Solar Cells. *Int. J. Mol. Sci.* **2020**, *21*, 1735. https://doi.org/10.3390/ijms21051735.

44. Risi, G.; Becker, M.; Housecroft, C.E.; Constable, E.C. Are Alkynyl Spacers in Ancillary Ligands in Heteroleptic Bis(Diimine)Copper(I) Dyes Beneficial for Dye Performance in Dye-Sensitized Solar Cells? *Molecules* **2020**, *25*, 1528. https://doi.org/10.3390/molecules25071528.

45. Inomata, T.; Hatano, M.; Kawai, Y.; Matsunaga, A.; Kitagawa, T.; Wasada-Tsutsui, Y.; Ozawa, T.; Masuda, H. Synthesis and Physico-Chemical Properties of Homoleptic Copper(I) Complexes with Asymmetric Ligands as a Dssc Dye. *Molecules* **2021**, *26*, 6835. https://doi.org/10.3390/molecules26226835.

46. Zhang, H.; Wu, X.; Tang, S.; Wang, K.; Tian, Y.; Zhong, C. Novel Metal Complexes for D-(A-π-A)2 Motif Dye Sensitizer: Synthesis and Photovoltaic Application. *Appl. Organomet. Chem.* **2021**, *35*, e6220. https://doi.org/10.1002/aoc.6220.

47. Franchi, D.; Leandri, V.; Pizzichetti, A.R.P.; Xu, B.; Hao, Y.; Zhang, W.; Sloboda, T.; Svanström, S.; Cappel, U.B.; Kloo, L.; et al. Effect of the Ancillary Ligand on the Performance of Heteroleptic Cu(I) Diimine Complexes as Dyes in Dye-Sensitized Solar Cells. *ACS Appl. Energy Mater.* **2022**, *5*, 1460–1470. https://doi.org/10.1021/acsaem.1c02778.

48. Tian, Y.; Wang, K.; Zhang, H.; Wu, X.; Zhong, C. Novel Polymeric Metal Complexes of Salicylaldehyde Schiff Base Derivative Being Used for Dye Sensitizer. *Tetrahedron* **2022**, *113*, 132756. https://doi.org/10.1016/j.tet.2022.132756.

49. Zhang, H.; Wu, X.; Tian, Y.; Wang, K.; Tang, S.; Zhong, C. Novel Polymeric Metal Complexes for Dye Sensitizer: Synthesis and Photovoltaic Performances. *J. Inorg. Organomet. Polym.* **2022**, *32*, 1736–1743. https://doi.org/10.1007/s10904-021-02220-w.

50. Çakar, S. 1,10 Phenanthroline 5,6 Diol Metal Complex (Cu, Fe) Sensitized Solar Cells: A Cocktail Dye Effect. *J. Power Sources* **2019**, *435*, 226825. https://doi.org/10.1016/j.jpowsour.2019.226825.

.